Gene therapy with secreted acid alpha-glucosidase rescues Pompe disease in a novel mouse model with early-onset spinal cord and respiratory defects

Pasqualina Colella, Pauline Sellier, Manuel J Gomez, Maria G Biferi, Guillaume Tanniou, Nicolas Guerchet, Mathilde Cohen-Tannoudji, Maryse Moya-Nilges, Laetitia van Wittenberghe, Natalie Daniele, et al.

EBioMedicine 61 (2020) 103052

Contents lists available at ScienceDirect

EBioMedicine

journal homepage: www.elsevier.com/locate/ebiom

Research paper

Gene therapy with secreted acid alpha-glucosidase rescues Pompe disease in a novel mouse model with early-onset spinal cord and respiratory defects

Pasqualina Colella[a,*], Pauline Sellier[a], Manuel J. Gomez[b], Maria G. Biferi[c], Guillaume Tanniou[a], Nicolas Guerchet[a], Mathilde Cohen-Tannoudji[c], Maryse Moya-Nilges[d], Laetitia van Wittenberghe[a], Natalie Daniele[a], Bernard Gjata[a], Jacomina Krijnse-Locker[d], Fanny Collaud[a], Marcelo Simon-Sola[a], Severine Charles[a], Umut Cagin[a], Federico Mingozzi[a,c,e,*]

[a] INTEGRARE, Genethon, Inserm, Univ Evry, Université Paris Saclay, Evry, France
[b] Bioinformatics Unit, CNIC, Madrid, Spain
[c] University Pierre and Marie Curie Paris 6 and INSERM U974, Paris, France
[d] Pasteur Institute, Paris, France
[e] Spark Therapeutics, Philadelphia, PA, USA

ARTICLE INFO

Article History:
Received 15 June 2020
Revised 2 September 2020
Accepted 15 September 2020
Available online 9 October 2020

Keywords:
Pompe disease
Mouse model
Respiratory function
Spinal cord
Muscle
AAV

ABSTRACT

Background: Pompe disease (PD) is a neuromuscular disorder caused by deficiency of acidalpha-glucosidase (GAA), leading to motor and respiratory dysfunctions. Available *Gaa* knock-out (KO) mouse models do not accurately mimic PD, particularly its highly impaired respiratory phenotype.
Methods: Here we developed a new mouse model of PD crossing *Gaa* KO$^{B6;129}$ with DBA2/J mice. We subsequently treated *Gaa* KO$^{DBA2/J}$ mice with adeno-associated virus (AAV) vectors expressing a secretable form of GAA (secGAA).
Findings: Male *Gaa* KO$^{DBA2/J}$ mice present most of the key features of the human disease, including early lethality, severe respiratory impairment, cardiac hypertrophy and muscle weakness. Transcriptome analyses of *Gaa* KO$^{DBA2/J}$, compared to the parental *Gaa* KO$^{B6;129}$ mice, revealed a profoundly impaired gene signature in the spinal cord and a similarly deregulated gene expression in skeletal muscle. Muscle and spinal cord transcriptome changes, biochemical defects, respiratory and muscle function in the *Gaa* KO$^{DBA2/J}$ model were significantly improved upon gene therapy with AAV vectors expressing secGAA.
Interpretation: These data show that the genetic background impacts on the severity of respiratory function and neuroglial spinal cord defects in the *Gaa* KO mouse model of PD. Our findings have implications for PD prognosis and treatment, show novel molecular pathophysiology mechanisms of the disease and provide a unique model to study PD respiratory defects, which majorly affect patients.
Funding: This work was supported by Genethon, the French Muscular Dystrophy Association (AFM), the European Commission (grant nos. 667751, 617432, and 797144), and Spark Therapeutics.

1. Introduction

Pompe disease (PD) or glycogen storage disease type II (GSDII, OMIM #232300) is a rare (~1 in 40,000 births) autosomal recessive condition caused by mutations in the gene encoding acid alpha-glucosidase (GAA), a constitutive lysosomal hydrolase converting glycogen to glucose [1, 2]. GAA deficiency leads to pathological glycogen accumulation that mainly affects the neuromuscular system [1–4]. Based on the onset and severity of pathological manifestations, PD is broadly categorized in classical infantile-onset PD (IOPD) and late-onset PD (LOPD) [1]. IOPD is caused by severe GAA deficiency (GAA activity < 1%) and presents at birth with cardiac hypertrophy, muscle hypotonia and severe respiratory impairment, leading to premature death, if not treated [5]. LOPD is characterized by diverse levels of residual GAA activity (up to ~20%) and can present in children and adults with proximal muscle weakness, motor and respiratory deficit, while

* Corresponding author at: INTEGRARE, Genethon, Inserm, Univ Evry, Université Paris-Saclay, Evry, France.
E-mail addresses: pcolella@stanford.edu (P. Colella), federico.mingozzi@sparktx.com (F. Mingozzi).

https://doi.org/10.1016/j.ebiom.2020.103052

Research in Context

Evidence before this study

Pompe disease (PD) is a metabolic neuromuscular disorder caused by the deficiency of the lysosomal enzyme acid alpha-glucosidase (GAA), which leads to pathological glycogen accumulation in virtually every cell of the body. Based on onset and severity, PD is broadly categorized in: classical infantile-onset PD (IOPD) and late-onset PD (LOPD). Respiratory insufficiency represents the most life-threatening manifestation and the leading cause of morbidity in IOPD and LOPD, in addition to IOPD-specific cardiomyopathy. Available *Gaa*-deficient mouse models of PD mostly lack a respiratory phenotype and show late-onset neuropathology, thus limiting research efforts towards the characterization and treatment of PD respiratory and neurological defects. Previous studies have shown that the genetic background modifies the severity of muscle phenotype in *Gaa*-deficient mice, a feature of PD that can be found also in affected humans. For example, *Gaa* knock-out (KO) mice in a C57BL/6;129;FVB background showed milder muscle disease compared to mice in a C57BL/6;129 background (abbreviates as Gaa KO$^{B6;129}$). Other studies have reported that the DBA2/J background increases the severity of muscular dystrophy (MD) in mice. The *Latent TGF-β–binding protein 4* (*Ltbp4*), a modifier gene present in the DBA2/J background, was also found to be a relevant genetic variant in human diseases, such Duchenne Muscular Dystrophy (DMD).

Added value of this study

In our study we show that the DBA2/J background worsens the phenotype of the *Gaa* KO mouse model of PD. Specifically, Gaa KO mice in a C57BL/6;129;DBA2/J background (abbreviates as Gaa KO^{DBA}) showed more severe respiratory defects and more profoundly altered spinal cord transcriptome than Gaa KO$^{B6;129}$, possibly associated with reduced survival. The Gaa KO^{DBA} mouse also presented all key PD disease manifestations including cardiac hypertrophy and muscle weakness, which provides a unique and stringent model of the disease. The activation of neuroinflammation, neuronal cell death, and pathological demyelination and remyelination processes found in the Gaa KO^{DBA} spinal cord also possibly explains muscle stimulation defects and white matter abnormalities observed in PD patients, which are linked with respiratory defects and cognitive abnormalities, respectively.

Implications of all the available evidence

While a treatment based on enzyme replacement therapy (ERT) is available, PD remains an unmet medical need, particularly when considering the rescue of respiratory symptoms and emerging central nervous system (CNS) manifestations, increasingly documented in IOPD. Our work provides a unique and highly stringent animal model to test the efficacy of novel therapies aimed at improving key PD manifestations. It also provides novel insight to the understanding of molecular mechanisms underlying neuromuscular disease and the crosstalk between the muscular and nervous system and suggests a role for *Latent TGF-β–binding protein 4* (*Ltbp4*) as possible modifier gene for PD. Finally, the correction of skeletal muscle and spinal cord transcriptome changes (90.5% and 62.5% of genes, respectively) and the improvement of the respiratory function of symptomatic Gaa KO^{DBA}, following gene transfer with investigational AAV vectors expressing secretable GAA, support the therapeutic potential of this approach for PD.

cardiac disease is typically absent [3,4]. Due to the diverse onset and severity of disease manifestations in LOPD subjects carrying the same *GAA* mutation, several studies have also suggested the impact of modifying factors on PD phenotype [6,7]. For example, cis-acting single nucleotide polymorphism (SNP) in the *GAA* gene and trans-acting polymorphisms in the *angiotensin-converting enzyme* (*ACE*) and *alpha Actinin 3* (*ACTN 3*) genes have been reported to impact on the disease onset in LOPD [8–10]. However, the *ACE* polymorphism did not justify the heterogeneity of disease onset and response to treatment in other LOPD cohorts [11,12]. The identification of PD modifying factors, still mostly unknown, would therefore represent an important step forward in the understanding of PD, allowing to improve both its prognosis and treatment.

The availability of the *Gaa* knock-out (KO) mouse [13], the most used animal model of PD, has been crucial to study and characterize the disease pathophysiology, the underlying molecular mechanisms, disease biomarkers and, not least, to test therapeutic approaches [14, 15]. The most severe and used *Gaa* KO mouse model was generated by Raben and colleagues in a mixed C57BL/6;129 background (Gaa$^{6neo/6neoB6;129-Gaatm1Rabn/J}$; abbreviated in this study as Gaa KO$^{B6;129}$) [13] and recapitulates key PD features like the i. whole body glycogen accumulation (including cardiac muscle, skeletal muscle and nervous tissue) [13,16]; ii. impaired autophagic flux in skeletal muscle [17,18]; iii. neuropathology [19–21]; iv. cardiac defects [22]; v. and muscle weakness [13,18]. However, despite being *Gaa* null, the Gaa KO$^{B6;129}$ mouse shows late onset, slowly progressive muscle weakness, mildly affected locomotor activity [13], and normal breathing in normoxic conditions [18,21,22]. In particular, the lack of important respiratory defects represents a key limitation of the Gaa KO$^{B6;129}$ mouse as model for PD [18,21,22], and hypercapnia has been widely exploited to challenge the respiratory phenotype [23–27]. Respiratory insufficiency indeed represents the most life-threatening disease manifestation and the leading cause of morbidity in both IOPD and LOPD [5,28–32], despite the advent of Enzyme Replacement Therapy (ERT) with recombinant human GAA (rhGAA) [14]. ERT, typically consisting of bi-weekly intravenous infusions of rhGAA, is the standard of care for PD since 2006 [14]. However, while ERT allows to extend the lifespan of IOPD subjects by effectively addressing the cardiac disease, and stabilizes disease progression in LOPD [14], it provides small benefits to the PD respiratory phenotype [5,14,32–37]. Additionally, white matter abnormalities and varied cognitive decline have emerged as secondary disease traits in long survivor IOPD subjects undergoing ERT [38,39]. The short plasma half-life of rhGAA, its inefficient uptake in key affected tissues, such as skeletal muscle and nervous tissue, and its high immunogenicity, are some of the hurdles that currently limit ERT efficacy [40,41].

In the present study, we report the generation, characterization, and phenotypic rescue of a novel Gaa KO mouse model of PD that recapitulates the main key disease manifestations in humans, including severe respiratory impairment at early age. The novel mouse model was generated by exploiting the DBA2/J genetic background and in particular, the *Latent TGF-β–binding protein 4* (*Ltbp4*) modifier gene, which has been described to act as a modulator of the severity of dystrophies in mice [42,43] and humans [44–46]. Interestingly, the observed severe respiratory phenotype in the novel Gaa KO model was accompanied with early and profound transcriptome changes in the spinal cord, supporting a substantial role of neurological involvement in the aetiology of PD. Using this model, we showed that the restoration of GAA enzyme activity by optimized adeno-associated virus (AAV) vector gene transfer [21,47] effectively improves the disease phenotype. Our study describes a stringent mouse model of PD, and provides novel insights into pathogenetic mechanisms, biomarkers, and potential novel therapeutic approaches to the disease.

2. Methods

2.1. Mouse studies

2.1.1. Mouse model

The original *Gaa* knock-out mouse strain (Gaa$^{6neo/6neoB6;129-Gaatm1-Rabn/J}$ also known as *Gaa*$^{6neo/6neo}$) [13] was purchased (Jackson Laboratory, MSR Cat# JAX:004154, RRID:IMSR_JAX:004154) and thoroughly characterized in our previous works [21,47,48]. Wild type DBA2/J mice were purchased (Jackson Laboratory, MSR Cat# JAX:000671, RRID: IMSR_JAX:000671). The original *Gaa* knock-out mouse strain (abbreviated in this work as Gaa$^{B6;129}$) was crossed with DBA2/J mice to generate the novel Gaa mouse strain homozygous for the *Ltbp4*$^{\Delta 36}$ allele (abbreviated in this work as Gaa^{DBA}). Details about mouse breeding and selection are depicted in Supplementary Figure S1a. Crossing of *Gaa*$^{+/-}$ *Ltbp4*$^{\Delta 36/\Delta 36}$ x *Gaa*$^{+/-}$ *Ltbp4*$^{\Delta 36/\Delta 36}$ was used to maintain the colony. Littermate mice were used, either affected (Gaa KO) or healthy (Gaa WT) from the two different strains: Gaa WT^{DBA} vs. Gaa KO^{DBA} and Gaa WT$^{B6;129}$ vs. Gaa KO$^{B6;129}$ (Fig. S1a). Mice were housed in Center for Exploration and Experimental Functional Research facility (CERFE, Evry, France) in a pathogen-free environment.

Study design. Mouse experimental groups were sized at n≥2; based on data generated in previous studies [21,47] all the samples/animals analysed were included in the data and none was excluded. For each data set, the exact number of mice (n), age, sex and genotype are detailed in the respective figure legend. To characterize the phenotype of male and female Gaa KO^{DBA} mice, sex- and age-matched Gaa WT^{DBA} mice were used as controls. Readouts of the study were non-invasive functional tests (grip test, plethysmography, rotarod and wire hang), quantitative biochemical analyses (glycogen content, Western blot for biomarkers) and tissue weight. Histological and RNA-seq analyses of muscle and spinal cord were performed in age-matched male mice. The endpoint of 4-5 months was selected to assess and compare adult mice before the death of an important fraction of male affected animals. To compare the phenotype of Gaa^{DBA} mice to the original Gaa$^{B6;129}$ strain, sex- and age-matched Gaa WT$^{B6;129}$ and Gaa KO$^{B6;129}$ were used. Gene therapy was performed in age-matched male Gaa^{DBA} mice. The random allocation of mice to the experimental groups (WT vs. KO) was driven by Mendelian inheritance, the date of birth and sex were the variables considered to generate control and treatment groups. Neonate animals from separate litters were randomised to the treatment groups at postnatal day 1 (untreated WT, vs untreated KO vs. AAV-secGAA administered KO) to have an n>3, n<5 mice/group, representative of the different litters, and each animal was assigned a random number from 1 to 13. Readouts of the study were quantitative biochemical analyses (glycogen assay, Western blot for human GAA and biomarkers) and gene expression analyses (RNA-seq; 3 mice/group, randomly selected). Adult animals from separate litters were randomised to the treatment groups at 2 months of age (untreated WT vs. untreated KO vs. AAV-secGAA administered KO) to have an n=5 mice/group, representative of the different litters; each animal was assigned a random number from 1 to 15. The AAV vector administration was performed by the same operator to minimise potential confounders. The study of mouse survival was performed based the observation of the Gaa^{DBA} and Gaa$^{B6;129}$ colonies over the indicated time periods. Late endpoints (6-10 months) were used during the manuscript revision phase to evaluate the respiratory phenotype of Gaa$^{B6;129}$ in comparison to sex- and age-matched Gaa^{DBA}, as Gaa$^{B6;129}$ have been reported to have a mild late-onset respiratory phenotype [21]. The experimenters were blind to group assignment during data generation and collection for all the experiments.

2.1.2. Mouse genotype

Genotyping for the *Gaa* allele was performed by PCR on genomic DNA following Protocol 23640 (Jackson Laboratory, Genotyping Protocols Database) and the following primers: GaaEx6 5'-ATGTCATCCTGCAACCCAG-3', oIMR7077 5'-ATTGTTGCACAACGCTCTTG-3', and oIMR7297 5'-CGTTGGCTACCCGTGATATT-3'. PCR products were analysed by gel electrophoresis using 1.5% agarose. Genotyping of the *Ltbp4* allele was performed by PCR on genomic DNA using the following primers: DBA2/J-Fw 5′- GGCTTTCTGCCTACTCGTCG -3′ and DBA2/J-Rev 5′- CCCGCAACCAACCTCTGATTC-3′. PCR products were analysed by gel electrophoresis using 3% agarose.

2.1.3. AAV delivery and sample collection

AAV2/9 vectors (abbreviated ad AAV9) were delivered to: 1. adult mice via the tail vein in a volume of 0.2 mL; 2. neonate mice at postnatal day 2 via the temporal vein in a volume of 0.03 mL. The AAV stock preparation was diluted in 0.001% Pluronic acid as surfactant (Thermo Fisher Scientific, Waltham, MA). All of animals were anesthetized and perfused with PBS before sacrifice; the operators that harvested samples from mice were blind to the sample group allocation.

2.2. Ethics

Mouse studies were performed according to the French and European legislation on animal care and experimentation (2010/63/EU) and approved by the institutional ethics committee of the Centre for Exploration and Experimental Functional Research facility (CERFE, Evry, France; protocols 2015-008, 2016-019).

2.3. Measurement of GAA activity and glycogen content

Snap-frozen tissues were homogenized in UltraPure™ DNase/RNase-Free Distilled Water (Thermo Fisher Scientific, Waltham, MA), using FastPrep lysis tubes (2 mL, 116910500, MP Biomedicals, Irvine, CA) according to manufacturer's instructions (1 min, 6 m/s) and tissue debris was removed by centrifugation 10 min at 10,000 x g. GAA activity was measured as previously described [49]. Briefly, the enzymatic reaction was set up using 10 μL of tissue homogenate appropriately diluted and 20 μL of 3 mM 4-methyl-umbelliferyl-α-d-glucoside substrate (4MUα-D-glucoside, Sigma Aldrich, Saint Louis, MO) in Sodium Acetate pH 4.65. The reaction mixture was incubated at 37 °C for one hour in black 96-well plates (PerkinElmer, Waltham, MA), and then stopped by adding 150 μl of Sodium Carbonate buffer pH 10.5. A standard curve (0−2500 pmol/μl of 4MU) was used to measure released fluorescent 4MU from individual reaction mixture in duplicate, using the EnSpire alpha plate reader (2390-0000, Perkin-Elmer, Waltham, MA) at 449 nm (Emission) and 360 nm (Excitation). The protein concentration of the tissue homogenates was quantified using the BCA Protein Assay (Thermo Fisher Scientific, Waltham, MA). To calculate the GAA activity, released 4MU concentration in each sample was divided by the respective protein concentration and activity was reported as nmol/hour/mg protein. Glycogen content was measured indirectly in tissue homogenates as the glucose released after total digestion with *Aspergillus Niger* amyloglucosidase (Sigma Aldrich, Saint Louis, MO). Samples were incubated for 5 min at 95 °C and then cooled at 4 °C; 25 μL of amyloglucosidase diluted 1:50 in 0.1 M potassium acetate pH 5.5 were then added to each sample. A control reaction without amyloglucosidase was prepared for each sample. Both sample and control reactions were incubated at 37 °C for 90 min. The reaction was stopped by incubating samples for 5 min at 95 °C. The glucose released was determined using a glucose assay kit (Sigma Aldrich, Saint Louis, MO) and by measuring resulting absorbance with the EnSpire alpha plate reader (Perkin-Elmer, Waltham, MA) at 540 nm.

2.4. Western blot analyses

Snap-frozen tissues were homogenized in UltraPure™ DNase/RNase-Free Distilled Water (Thermo Fisher Scientific, Waltham, MA),

using FastPrep lysis tubes (2 mL, 116910500, MP Biomedicals, Irvine, CA) as described above. Protein concentration was determined using the BCA Protein Assay (Thermo Fisher Scientific, Waltham, MA). SDS-page electrophoresis was performed in a 4-15% gradient polyacrylamide gel. After transfer, the membrane was blocked with Odyssey buffer (Li-Cor Biosciences, Lincoln, NE) and incubated with an anti-human GAA antibody (Cat# ab137068, RRID:AB_2687584, rabbit monoclonal, Abcam, Cambridge, MA), anti-p62 (Cat# ab56416, RRID: AB_945626 mouse monoclonal, Abcam, Cambridge, MA), anti-Vinculin (Cat# V9131, RRID:AB_477629, mouse monoclonal, Sigma Aldrich, Saint Louis, MO), anti-Gapdh (Cat# PA1-988, RRID:AB_2107310, rabbit polyclonal, Thermo Fisher, Waltham, MA), anti-Parkin (ab77924, mouse monoclonal, Abcam, Cambridge, MA), anti LC3b (Cat# sNB-100-2220, RRID:AB_10003146, rabbit polyclonal, Novus Biologicals) . The membrane was washed and incubated with the appropriate secondary antibody (Li-Cor Biosciences), and visualized by Odyssey imaging system (Li-Cor Biosciences). Band intensity was quantified by ImageJ software.

2.5. Histological evaluation

For muscle histology, immediately after euthanasia heart, diaphragm, quadriceps and triceps brachii were snap-frozen in isopentane (−160 °C) previously chilled in liquid nitrogen. Serial 8 μm cross-sections were cut in a Leica CM3050 S cryostat (Leica Biosystems). To minimize sampling error, 2−3 sections of each specimen were obtained and stained with haematoxylin-eosin (HE) or and periodic acid-Schiff (PAS) according to standard procedures. Muscle images were acquired using an Axioscan slide scanner (ZEISS, Munich, Germany), using a plan-apochromat 10x magnitude 0.45 NA objective. For spinal cord histology, after being explanted spinal cords were fixed in 4% PFA and then transferred in a 30% PBS-sucrose solution. Spinal cords were divided in cervical, thoracic and lumbar segments and then embedded in Tissue-Tek OCT (Sakura Finetek, Alphen aan den Rijn, the Netherlands), and frozen in cold isopentane (−50 °C). Fourteen micrometre-thick cryosections were serially cut using a cryostat (Leica Biosystems, Nussloch, Germany). Spinal cord sections were fixed with 4% PFA, permeabilized in 0.1% Triton X-100 in PBS and stained with the primary antibodies: anti-ChAT (Choline acetyltransferase, Cat# AB144P, RRID:AB_2079751, Merck Millipore, Billerica, MA), rabbit anti GFAP (glial fibrillary acidic protein, Cat# Z0334, RRID:AB_10013382, Agilent Technologies, Santa Clara, CA). After washing, tissues were incubated with the appropriate fluorescent-dye conjugated secondary antibodies (Thermo Fisher Scientific, Waltham, MA) combined with 4′,6-diamidino-2-phenylindole (DAPI) staining. ChAT-positive motor neurons (with a diameter $>$ 20 μm) were manually counted in the grey matter of the cervical spinal cord segments using an epifluorescence microscope (Leica Microsystems, Buffalo Grove, IL). A total of 24 sections per mouse were counted in the entire cervical spinal cord (regions C1−C7), the 24 counted sections were distributed in 3 separate serial slides (8 sections/slide). Periodic acid-Schiff (PAS) staining was performed according to standard procedures using in the entire cervical spinal cord (C1−C7; 20 sections/mouse). Astroglial reaction was evaluated by measuring the fluorescence intensity of the GFAP staining in the grey matter of the spinal cords using the ImageJ software. The operators performing cell counting and morphological analyses were blind to the sample group allocation.

2.6. Electron microscopy analyses

Muscle samples were fixed with 2.5% glutaraldehyde (Sigma Aldrich, Saint Louis, MO) in 0.1M PHEM buffer, pH 7.2 immediately after euthanasia. Post fixation was done with 1% osmium tetroxide (Merck) and 1.5% ferrocyanide (Sigma Aldrich, Saint Louis, MO) in 0.1 M Hepes. After dehydration by a graded series of ethanol, the tissue samples were infiltrated with epoxy resin. Polymerized resin blocks were thin sectioned longitudinally using a Leica UC 7 microtome (Leica microsystems). The 70 nm sections were collected on formvar coated slot grids (EMS) and were contrasted with 4% uranyl acetate and Reynolds lead citrate. Stained sections were observed with a Tecnai spirit FEI operated at 120 kV. Images were acquired with FEI Eagle digital camera. The quantification of lysosome length was performed as previously described [50] using ImageJ software. Lysosomes were measured in multiple sections for a total of 10 fields (Gaa KO^{DBA}) and 25 fields (Gaa KO$^{B6;129}$). The operator performing the lysosome measurements was blind to the sample group allocation.

2.7. Functional mouse analyses

Respiratory function during quiet breathing was evaluated as already reported [21]. Briefly, a flow-through (0.5 L/min) plethysmograph (EMKA technologies, Paris, France) was used to measure the breathing pattern in mice. Before the assessment, the instrument was calibrated with known airflow and pressure signals for optimal data collection. Signals were analysed using the IOX2 software (EMKA technologies). Animals were allowed for acclimation into the plethysmograph chamber before testing. During both acclimation and data acquirement, mice were breathing normoxic air (21% O2, 79% N2). Forelimbs wire-hanging test was performed as already reported [21]. A 4-mm wire was used to record the number of falls over a period of 3 minutes. The number of falls per minute was reported. Rotarod coordination test was performed as already reported [21] using a LE8200 apparatus (Harvard Apparatus, Holliston, MA). An accelerating protocol 4−40 rpm in 5 min was used. The test was repeated three times, the maximum and average time spent on rod for each animal was reported. A null time represents the inability of mice to stand on the rod even at the minimum acceleration used (4 rmp). Grip strength was measured using a grip strength meter, (Bioseb Grip test 25N) as previously reported [21]. Briefly three independent measurements of the four limbs strength were averaged. Mean values of grip strength were reported. The operators performing the tests were blind to the mouse group allocation.

2.8. RNA Isolation, RNA-seq library construction and sequencing

Total RNA was isolated from snap-frozen quadriceps muscle and whole spinal cord preserved at −80 °C. Samples were homogenized in Trizol and total RNA was purified on-column using the PureLink™ RNA Mini Kit (Invitrogen, Waltham, MA) according to manufacturer's protocol and including an on-column DNase digest (PureLink™ DNase Set DNAse set, Invitrogen, Waltham, MA). All samples used for RNA-seq were randomized and processed in parallel to reduce extraction variability. The quality of the extracted RNA was evaluated using the Agilent 2100 Bioanalyzer and the Eukaryote Total RNA Nano chip (Agilent, Santa Clara, CA). 200 ng of total RNA were used to generate barcoded RNA-seq libraries using the NEBNext Ultra RNA Library preparation kit (New England Biolabs, Ipswich, MA). Briefly, poly A+ RNA was purified using poly-T oligo- attached magnetic beads followed by fragmentation and then first and second cDNA strand synthesis. Next, cDNA 3' ends were adenylated and the adapters were ligated followed by PCR library amplification. Finally, the size of the libraries was checked using the Agilent 2100 Bioanalyzer DNA 1000 chip and their concentration was determined using the Qubit® fluorometer (Life Technologies). Libraries were sequenced on a HiSeq2500 (Illumina) to generate 60 bases single reads. FastQ files for each sample were obtained using CASAVA v1.8 software (Illumina).

2.9. Bioinformatics analysis of RNA-seq data

RNA-seq data analysis was performed by the Bioinformatics Unit of Centro Nacional de Investigaciones Cardiovasculares (CNIC, Madrid, Spain). Sequencing reads were processed with a pipeline that used FastQC to evaluate their quality (http://www.bioinformatics.babraham.ac.uk/projects/fastqc/, developed by Babraham Institute), and cutadapt to trim sequencing reads, eliminating Illumina adaptor remains, and to discard reads that were shorter than 30 bp. Resulting reads were mapped against mouse transcriptome GRCm38.91, and gene expression levels were estimated with RSEM. Around 91% of the reads from any sample participated in at least one reported alignment. Expression count matrices were then processed with an analysis pipeline that used Bioconductor package limma for normalization [using the trimmed mean of M-values normalization (TMM) method] and differential expression testing, focusing on genes expressed with at least 1 count per million (CPM), in at least three samples. Changes in gene expression were considered significant if associated to Benjamini and Hochberg (BH) adjusted p-value < 0.05. To identify and classify groups of genes with different degrees of restored expression towards wild type levels after AAV treatment, we averaged expression values from untreated Gaa KO^{DBA}, Gaa WT^{DBA} and AAV-treated Gaa KO^{DBA} samples, in skeletal muscle and spinal cord, for collections of DEGs identified in contrast untreated Gaa KO^{DBA} vs. Gaa WT^{DBA}. DEGs were selected using abs(logFC) > 0.5, on top of the standard adjusted p-value < 0.05 filter. The resulting expression profiles, consisting of 2573 and 137 genes in skeletal muscle and spinal cord, respectively, were clustered using K-Means with n=6. Clusters with complementary expression profiles were combined to define three metaclusters. Each metacluster contained genes with expression levels that had been fully rescued, partially rescued or not rescued in animals receiving the AAV9-secGAA vector.

Differentially expressed and metacluster gene collections were processed with Ingenuity Pathway Analysis (IPA, Qiagen) to identify associations with Canonical Pathways, Diseases and Biofunctions. Functional associations provided by IPA are characterized by two parameters: p-values to describe enrichment test significance and z-scores to indicate predicted activation state. Enrichments were considered significant if associated to p-value < 0.05. Calculation of z-score for a given pathway, or regulator, is based on the fold change value of associated genes and can only be applied, by definition, to pairwise contrast results. Positive and negative z-scores suggest higher activity in the first or the second condition being compared, respectively. Abs(z-score) values higher than 2 are considered relevant. To identify potential changes in cell populations in both Gaa KO^{DBA} and Gaa KO$^{B6;129}$ spinal cords, we used CTen [51], an algorithm to perform enrichment analyses with a database of highly expressed, cell-type specific genes. Input files consisted in collections of 434 and 129 DEGs with logFC > 0.5, upregulated in Gaa KO^{DBA} and Gaa KO$^{B6;129}$, respectively, relative to their WT counterparts. Scores reported by CTen are Benjamini-Hochberg-adjusted enrichment p-values, and the recommended threshold of significance is -log10(BH p-value) >= 2. Lists of mouse genes associated to fibrosis, necrosis and inflammatory response were recovered from IPA's knowledgebase. Genes associated to muscular regeneration were recovered from Ensembl/BioMart, associated to GO term GO:0043403 (skeletal muscle tissue regeneration).

2.10. GAA expression cassettes and AAV vector generation

The GAA transgene expression cassettes containing the codon-optimized coding sequence encoding for the secretable form of human GAA were previously described [21,47]. The AAV9 vectors used in this study were produced using an adenovirus-free transient transfection method as described earlier [52]. Titres of AAV vector stocks were determined using quantitative real-time PCR (qPCR) and confirmed by SDS-PAGE followed by SYPRO Ruby protein gel stain and band quantification using ImageJ software. All vector preparations were quantified at least 2 times before use and tested in our previous work [47]. Two secGAA expression cassettes under the control of tandem promoters were selected based on our previous publication [47]. The LiNeuP (Liver Neuron Promoter: ApoE-hAAT-hSYN) [47] was used in adult mice (study depicted in Figs. 6 and 7) to restore GAA enzyme activity in muscle and spinal cord. The LiMP promoter (Liver Muscle Promoter: ApoE-hAAT-spC5.12) [47] was used in the study depicted in Figs. 4 and 5 based on its ability to drive long-term body-wide restoration of GAA enzyme activity in neonate mice. Conversely, due to AAV vector genome dilution, gene transfer with the LiNeuP promoter in neonate mice does not lead to long term systemic correction of PD [47]. The detailed characterisation of the LiNeuP and LiMP promoters is reported in Colella et al. [47].

2.11. Statistics

All the data showed in the present manuscript are reported as mean ± standard deviation of the mean. The number of sampled units, n, upon which we reported statistic is the single mouse for the in vivo experiments (one mouse is n = 1). GraphPad Prism 7 software (GraphPad Software) was used for statistical analyses. Parametric tests were used with data having a normal distribution (evaluated using the Shapiro–Wilk test). The statistical tests used were: unpaired Student's t-test for two-group comparisons, One-way ANOVA with Tukey post hoc for comparisons with more than two groups, Two-way ANOVA with Tukey or Sidak post-hoc for multiple variable comparisons. For all the data sets analysed by parametric tests, alpha=0.05. All statistical tests were performed two-sided. p-values <0.05 were considered significant. The statistical analysis performed for each data set is indicated in the figure legends. For all figures $^{*}p < 0.05$, $^{**}p < 0.01$, $^{***}p < 0.001$, $^{****}p < 0.0001$, $\#p < 0.05$, $\#\#p < 0.01$, $\#\#\#p < 0.001$, $\#\#\#\#p < 0.0001$.

2.12. Role of the funding source

The funders had no role in study design, data collection, data analyses, interpretation, or writing of report.

3. Results

3.1. Male Gaa KO mice homozygous for the Ltbp4$^{\Delta 36}$ allele show early lethality, reduced muscle strength and early respiratory impairment

To generate *Gaa*$^{-/-}$ mice homozygous for the *Ltbp4*$^{\Delta 36}$ allele, we crossed *Gaa*$^{-/-}$ mice from our original colony (having a mixed C57BL/6;129 background) [21] with wild type DBA2/J mice. Upon breeding and selection (Fig. S1a), we obtained mice that were homozygous for the *Ltbp4*$^{\Delta 36}$ allele and either wild type or knock-out for *Gaa: Gaa*$^{+/+}$ *Ltbp4*$^{\Delta 36/\Delta 36}$ (abbreviated as Gaa WT^{DBA}) or *Gaa*$^{-/-}$ *Ltbp4*$^{\Delta 36/\Delta 36}$ (abbreviated as Gaa KO^{DBA}), respectively (Fig. 1a). Mice from the original colony used in the present study as comparison were: *Gaa*$^{+/+}$ *Ltbp4*$^{+36/+36}$ (abbreviated as Gaa WT$^{B6;129}$) or Gaa$^{-/-}$ *Ltbp4*$^{+36/+36}$ (abbreviated as Gaa KO$^{B6;129}$) (Figs. 1a and S1b). Genotyping for the *Ltbp4* allele by PCR confirmed that all mice from the original *Gaa* mouse colony (Gaa$^{B6;129}$) were homozygous for the *Ltbp4*$^{+36}$ allele (Fig. S1c), as expected based on the B6;129 background [42]. Since we have observed that the PD phenotype in Gaa KO$^{B6;129}$ mice is less severe in females than males [48], in the present study we mainly focused on the phenotype of the latter. Upon establishing the colony (Figs. 1a and S1a), we observed that the survival of male Gaa KO^{DBA} was reduced compared to unaffected Gaa WT^{DBA} (~50% survival at 6 months of age, Fig. 1b). The mortality of male Gaa KO^{DBA} was anticipated compared to Gaa KO$^{B6;129}$ mice, which showed ~50% survival at 10 months of age (Fig. 1b), as observed in our previous Gaa$^{B6;129}$

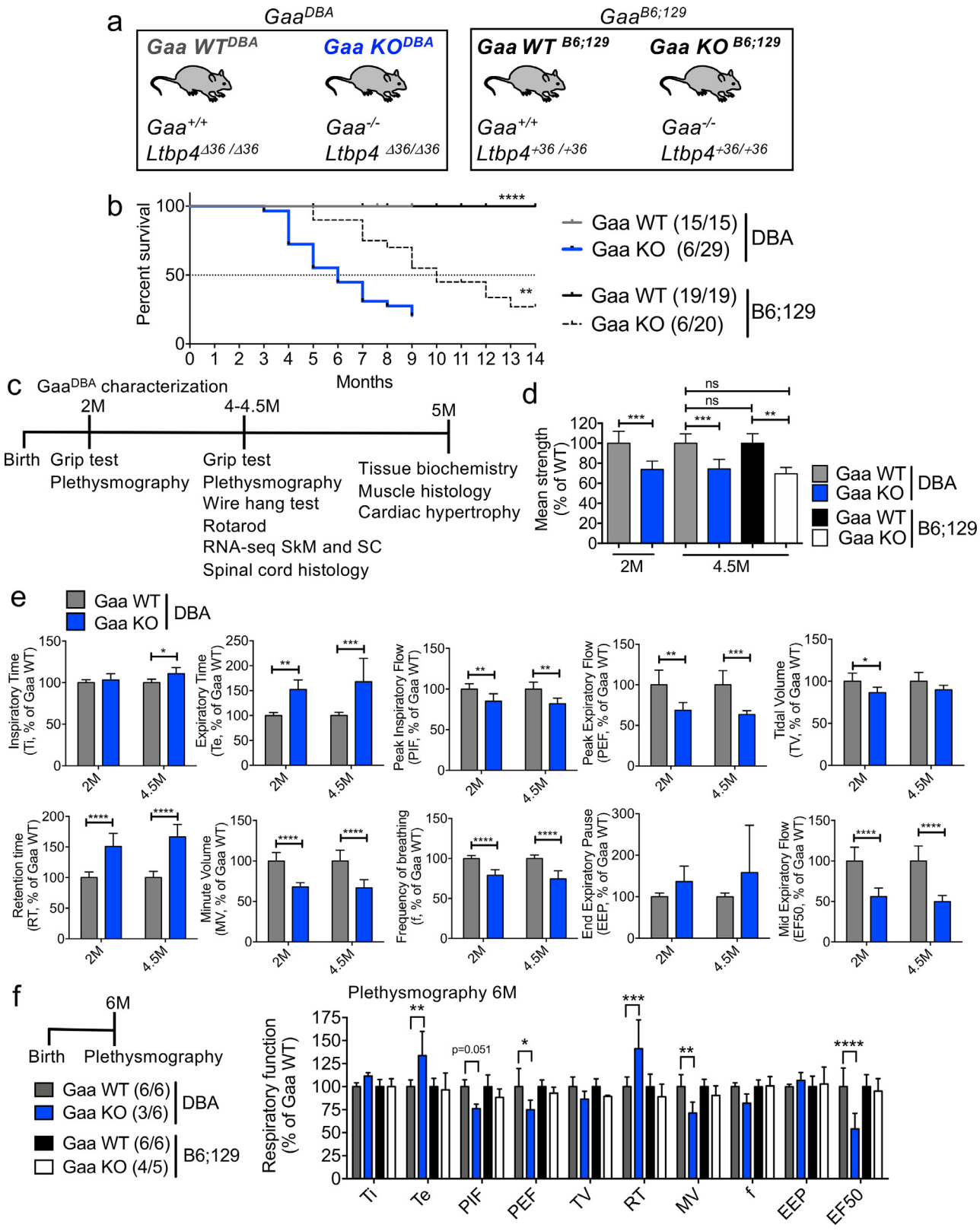

Fig. 1. Gaa KO^{DBA} mice show reduced survival, muscle weakness and early impairment of the respiratory function.(a) Gaa$^{+/+}$ Ltbp4$^{\Delta 36/\Delta 36}$ (abbreviated as Gaa WT^{DBA}) or Gaa$^{-/-}$ Ltbp4$^{\Delta 36/\Delta 36}$ (abbreviated as Gaa KO^{DBA}), Gaa$^{+/+}$ Ltbp4$^{+36/+36}$ (abbreviated as Gaa WT$^{B6;129}$) or Gaa$^{-/-}$ Ltbp4$^{+36/+36}$ (abbreviated as Gaa KO$^{B6;129}$) were used throughout the study. (b) Lifespan curve of male Gaa^{DBA} and Gaa$^{B6;129}$ mice during the observation time, the number of alive mice out of total analysed is depicted in brackets. (c) Diagram for the 5-month Gaa^{DBA} characterization study. SkM: skeletal muscle; SC: spinal cord. (d) Muscle strength measured by 4-limb grip strength test in male Gaa^{DBA} at 2 months (2M) and 4.5 months (4.5M) of age; male Gaa$^{B6;129}$ at 4.5M were used as comparison. Percentage values relative to the respective Gaa WT controls are depicted. (e-f) Respiratory function measured by whole body plethysmography during quiet breathing in: (e) male Gaa^{DBA} mice at 2 and 4.5 months (M) of age, (f) male Gaa^{DBA} and Gaa WT^{DBA} at 6 months of age. Percentage values relative to the respective Gaa WT controls are depicted. (e-f) Inspiratory time (Ti), expiratory time (Te), peak inspiratory and expiratory flow (PIF, PEF, respectively), tidal volume (TV), retention time (RT), minute volume (MV), frequency of breathing (f), end expiratory pause (EEP), mid expiratory flow (EF50). (d-e) Gaa WT$^{DBA:}$ n = 7; Gaa KO^{DBA} n = 7 at 2 months, Gaa KO^{DBA} n = 6 at 4.5 months due to the death of 1 out of 7 mice. (d) Gaa WT$^{B6;129}$ n = 6 and Gaa KO$^{B6;129}$ n = 5. (f) The study diagram is depicted, the number of alive mice

studies [21,48]. We then evaluated muscle strength and respiratory function in male Gaa^{DBA} mice at 2 and 4.5 months of age (Fig. 1c–e), to perform the analyses in juvenile and adult mice, respectively, before the death of an important fraction of affected animals (Fig. 1b). A reduction in muscle strength of ~26% was observed at both time points in affected Gaa KO^{DBA} compared to Gaa WT^{DBA} (Fig. 1d). No significant differences in muscle strength were observed comparing the Gaa^{DBA} to the Gaa$^{B6;129}$ strain (Fig. 1d). A ~26.6% decrease in muscle strength in 4-month-old Gaa KO$^{B6;129}$ was also reported in our previous Gaa$^{B6;129}$ publications [21,47,48]. Importantly, we found that the respiratory function measured by whole-body plethysmography during quiet breathing, was significantly affected in male Gaa KO^{DBA} compared to Gaa WT^{DBA} (Fig. 1e and Table S1). Most of the plethysmography parameters were significantly altered in male Gaa KO^{DBA} mice compared to Gaa WT^{DBA} at 2 and 4.5 months, with no significant progression (Fig. 1e and Table S1). In particular, Gaa KO^{DBA} mice showed increased expiratory time (Te) and retention time (RT) while decreased peak inspiratory and expiratory flow (PIF, PEF), minute volume (MV), frequency of breathing (f) and mid expiratory flow (EF50) (Fig. 1e and Table S1). Plethysmography analyses at 6 months of age, when a sufficient number of Gaa KO^{DBA} mice were still alive, also showed statistically significant defects in Gaa KO^{DBA} but not Gaa KO$^{B6;129}$ (Fig. 1f). No statistically significant alteration of the respiratory function was measured in affected Gaa$^{B6;129}$ mice even at older ages (7 and 9 months) (Fig. S2a), consistent with what we observed in previous studies [21]. Interestingly, differently from Gaa KO$^{B6;129}$ mice, Gaa KO^{DBA} mice showed decreased performance in the rotarod test, suggesting coordination defects (Fig. S2b, Table S2) [53]. Conversely, hind limb strength measured by wire hang test was not significantly impaired in Gaa KO^{DBA} mice and Gaa KO$^{B6;129}$ (Fig. S2c, Table S2), as we observed in previous Gaa$^{B6;129}$ studies [21]. At the end of the characterization study (5 months, Fig. 1b), we confirmed pathological glycogen storage in muscle and nervous system of Gaa KO^{DBA} compared to Gaa WT^{DBA} (Fig. S3a). The measurement of glycogen storage also showed similar accumulation in tissues of Gaa KO^{DBA} vs. Gaa KO$^{B6;129}$ mice (Fig. S3b). Autophagy block, a hallmark of PD in skeletal muscle [17,54], was also readily observed by measuring the accumulation of p62 (Fig. S3c-d) and the ratio LC3bII/I (Fig. S3e-f), which together reflect the block of the autophagic flux [55]. Cardiac hypertrophy, another well-recognized phenotype of Gaa KO mice and IOPD subjects, was present in male Gaa KO^{DBA} compared to Gaa WT^{DBA} and was not different from that observed in Gaa KO$^{B6;129}$ (Fig. S3g, Table S3). During the observation period, the body weight of male Gaa KO^{DBA} remained stably lower than Gaa WT^{DBA} by ~14% (Table S3).

The survival of female Gaa KO^{DBA} and Gaa KO$^{B6;129}$ mice was not different from unaffected Gaa WT controls (Fig. S4a). Female Gaa KO^{DBA} showed a slight reduction in muscle strength (~18% at 4.5 months, Fig. S4b and c), which was not different compared to female Gaa KO$^{B6;129}$ (Fig. S4c). In the 5-month study, we observed a mild alteration of some respiratory parameters (Te, f and EEP; Fig. S4d, Table S4), glycogen storage in tissues (Fig. S4e), and no cardiac hypertrophy (Table S4). The long-term survival of female Gaa KO$^{B6;129}$ and Gaa KO^{DBA} mice (Fig. S4a) allowed us to do analyses at late time points. Plethysmography analyses at 9 months of age showed statistically significant alteration of respiratory parameters in Gaa KO^{DBA} but not Gaa KO$^{B6;129}$ females (Te, RT, MV, f, EEP and EF50; Fig. S4f). Late onset cardiac hypertrophy was also observed and was similar in female Gaa KO mice from both strains (Fig. S4g). Pathological glycogen accumulation was also not different in age-matched tissues of female Gaa KO^{DBA} and Gaa KO$^{B6;129}$ (Fig. S4h). These results emphasize the key unique features of the Gaa KO^{DBA} phenotype, in particular its increased severity in terms of respiratory defects and reduced survival in male mice.

3.2. Muscle is similarly affected in Gaa KO^{DBA} and Gaa KO$^{B6;129}$ mice

To further characterize the disease phenotype of Gaa KO^{DBA} in muscle, we performed histological (Fig. 2a), ultrastructural (Fig. 2b-c) and transcriptomic analyses (Fig. 2d–f) in male animals between 4 and 5 months of age. Cross-sections of quadriceps skeletal muscle stained by haematoxylin and eosin (HE) showed a similar structure when comparing unaffected (Gaa WT^{DBA} vs. Gaa WT$^{B6;129}$) and affected (Gaa KO^{DBA} vs. Gaa KO$^{B6;129}$) mice at 5 months of age (Fig. 2a), with no apparent signs of necrosis, fibrosis, calcification or important inflammatory infiltrates. Periodic acid Schiff (PAS) staining clearly reflected glycogen accumulation in quadriceps of Gaa KO^{DBA} and Gaa KO$^{B6;129}$ compared to the unaffected controls (Fig. 2a). Histological HE and PAS analyses of cardiac muscle, diaphragm and triceps from Gaa KO^{DBA} at 5 months also did not show any apparent defect other than glycogen and autophagic inclusions (Fig. S5a), similar to what also reported in the original Gaa KO$^{B6;129}$ mouse strain [21,56]. The diaphragm, which is important for the respiratory function, presented similar histology in 5-month-old Gaa KO^{DBA} and Gaa KO$^{B6;129}$ (Fig. S5a and b). High-resolution electron microscopy (EM) clearly revealed the presence of expanded lysosomes, a PD hallmark [57], only in the quadriceps of Gaa KO^{DBA} and Gaa KO$^{B6;129}$ mice but not Gaa WT^{DBA} and Gaa WT$^{B6;129}$ mice (Fig. 2b). The length of the expanded lysosomes did not differ in Gaa KO^{DBA} compared to Gaa KO$^{B6;129}$ (Fig. 2c). To evaluate the patterns of gene expression change in skeletal muscle of each mouse line, we performed transcriptome analyses by RNA sequencing (RNA-seq) of 4-month-old Gaa^{DBA} and Gaa$^{B6;129}$mice (Fig. 2d–f) and performed functional enrichment analyses with IPA (Ingenuity Pathway Analysis) on the collections of detected differentially expressed genes [DEGs, Benjamini and Hochberg (BH) adjusted p-value < 0.05]. A similar number of DEGs was detected in KO vs. WT comparisons of quadriceps samples from each of the two mouse lines: 6196 DEGs in Gaa KO^{DBA} vs. Gaa WT^{DBA}, and 6230 DEGs in Gaa KO$^{B6;129}$vs. Gaa WT$^{B6;129}$ (Fig. 2d). Notably, 52% of the DEGs were shared between the two mouse lines, suggesting a similar gene expression profile in diseased skeletal muscle (Fig. 2d). The activation profile of the most significantly enriched canonical pathways detected by IPA [BH p value < 0.05 and absolute (z score) >2, in at least one comparison] evidenced a similar disease-associated signature in the quadriceps of Gaa KO^{DBA} and Gaa KO$^{B6;129}$ mice (Fig. 2d). Interestingly, several of the pathways with the highest activation score values in Gaa KO mice are involved in the control of inflammation, immune response and oxidative stress (Fig. 2e). We then evaluated the differential expression of genes involved in known muscle pathological processes such as fibrosis, inflammatory response, muscle regeneration and necrosis (Fig. 2f, Fig. S6a). We found that expression change patterns were similar in KO vs. WT mice from each of the two lines (Fig. 2f). Accordingly, log fold change (logFC) values were highly correlated, with Pearson coefficients higher than 0.82 in all cases (Fig. S6a). Some example of genes similarly deregulated in affected mice from both colonies and involved in muscle degeneration and regeneration processes were foetal myosin heavy chains 8 and 3 (Myh8 and Myh3 with approximately 4 and 10 fold expression increments, respectively, in Gaa KO vs. Gaa WT, BH adjusted p-value<0.0001), Myogenin (MyoG, with approximately ~4–5 fold expression increase in Gaa KO vs. Gaa WT, BH adjusted p-value < 0.0001) and Klotho (Kl, with approximately 3–5 fold decrease, respectively, in Gaa KO vs. Gaa WT, BH adjusted p-value<0.01), and, apoptosis, like Caspase1, 3 and 6 (Casp1, 3 and 6, with

at 6 months out of total originally included in the study is depicted in brackets. (d-f) Data are depicted as average±SD. Statistical analyses: (b) Log-Rank (Mantel-Cox) test: **** p< 0.0001 (Gaa WT^{DBA} vs. Gaa KO^{DBA} and Gaa WT$^{B6;129}$ vs. Gaa KO$^{B6;129}$), ** $p < 0.01$ (Gaa KO^{DBA} vs. Gaa KO$^{B6;129}$); (d) One-way ANOVA with Tukey post-hoc; (e) Two-way ANOVA with Tukey post-hoc (genotype, age); (f) Multiple t-test with Holm-Sidak post-hoc. *$p < 0.05$, **$p < 0.01$, ***$p < 0.001$, ****$p < 0.0001$.

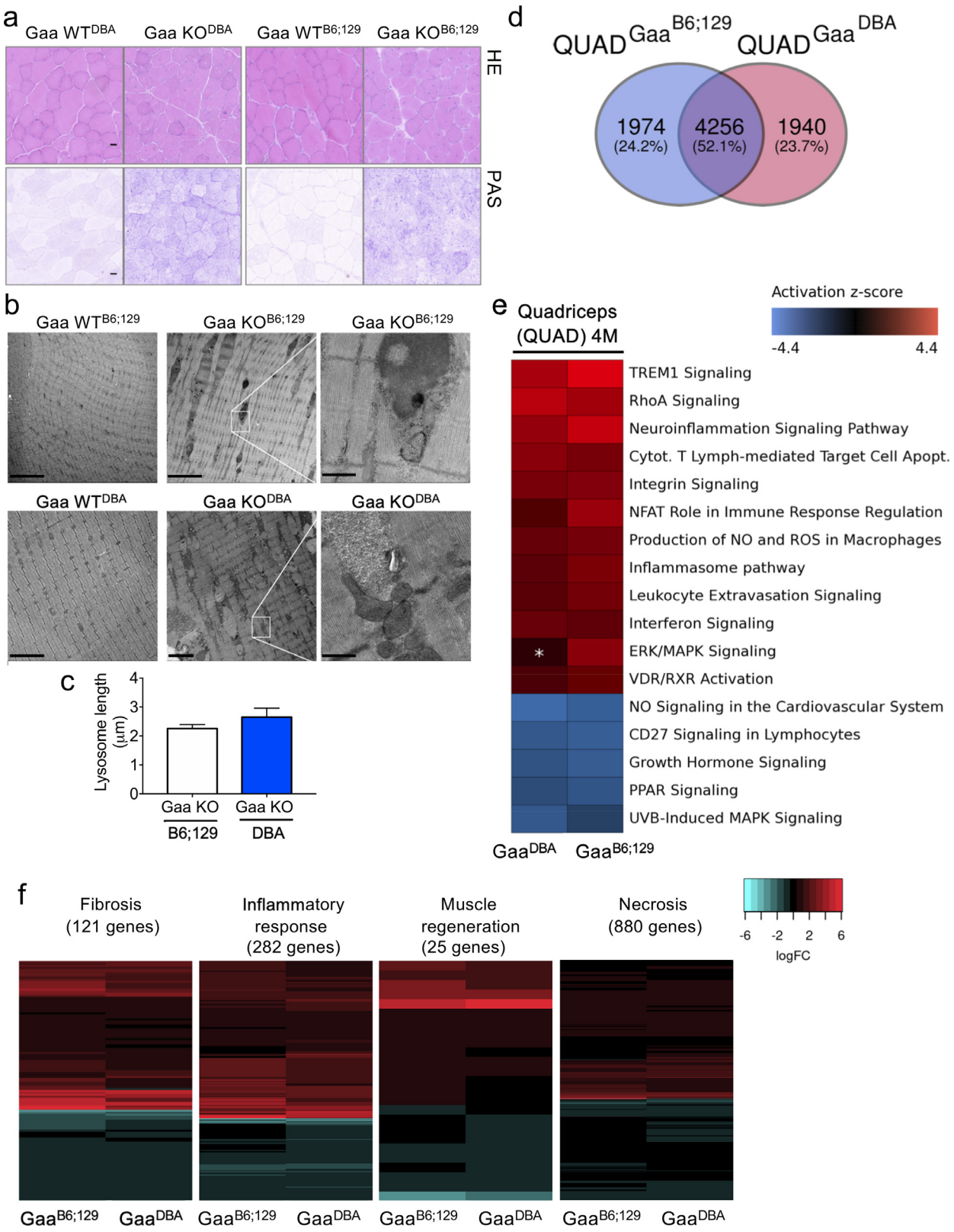

Fig. 2. Histological, ultrastructural and transcriptome analyses show a similarly affected skeletal muscle in Gaa KO^{DBA} and Gaa KO$^{B6;129}$ mice.(a) Haematoxylin-eosin (HE) and Periodic acid-Schiff (PAS) staining of quadriceps skeletal muscle from 5-month-old male Gaa^{DBA} and Gaa$^{B6;129}$ mice, n = 2 mice/sample. The scale bar is 20 μm. (b-c). Electron microscopy analysis of tibialis anterior skeletal muscle from 4-month-old male Gaa^{DBA} and Gaa$^{B6;129}$ mice; n = 2 mice/sample; the number of lysosomes measured was 55 (10 fields) for Gaa KO^{DBA}, and 172 (25 fields) for Gaa KO$^{B6;129}$ mice. The scale bar is 5 μm (left and middle panel), 500 nm (right panel). No expanded lysosomes are found in wild type mice (Gaa WT^{DBA} and Gaa WT$^{B6;129}$). (c) Data are depicted as average±SD. (d-f) Downstream analysis of RNA sequencing (RNA-seq) data obtained from the quadriceps skeletal muscle of 4-month-old male Gaa^{DBA} and Gaa$^{B6;129}$ mice. Expression data from 17420 genes with at least 1 count per million (CPM), in at least three samples, were used to evaluate differential expression in pairwise comparisons Gaa KO^{DBA} vs. Gaa WT^{DBA} and Gaa KO$^{B6;129}$ vs. Gaa WT$^{B6;129}$; n = 3 mice/sample. (d) Venn diagram distribution of specific and shared differentially expressed genes (DEGs), with Benjamini-Hochberg (BH) adjusted p-value < 0.05, in each of the comparisons. (e) Comparative view of Canonical Pathway analysis results obtained with Ingenuity Pathway Analysis (IPA) for each DEG collection. The heatmap shows a selection of pathways detected as significantly enriched (p-value < 0.05) in at least

approximately 2 fold expression increase in Gaa KO vs. Gaa WT, BH adjusted p-value<0.05). We then determined whether the changes in gene expression profiles observed here were similar to those found in related public datasets. We compared the collections of DEGs identified here in KO vs. WT contrasts in 4-month-old Gaa^{DBA} and Gaa$^{B6;129}$ mice, with those identified by Lim and colleagues in 5-month-old Gaa KO$^{B6;129}$ gastrocnemius and those previously identified by us in 18-month-old Gaa KO$^{B6;129}$ quadriceps [48] (Fig. S6b). The fraction of shared DEGs with logFC > 0.5 was 50% or higher in all pairwise comparisons, and logFC values for shared DEGs were highly correlated in all cases, with Pearson coefficient values above 0.78 (Fig. S6c and d), suggesting a high similarity between the transcriptome changes in Gaa^{DBA} and Gaa$^{B6;129}$ skeletal muscle. Overall, these results indicate that muscle is similarly affected in Gaa KO^{DBA} and Gaa KO$^{B6;129}$ mice, then they also provide novel insights into key pathways involved in muscle pathology in PD.

3.3. *Profoundly deregulated gene expression and motor neuron loss is observed in the spinal cord of Gaa KO^{DBA} mice*

Neurological defects caused by glycogen storage in the spinal cord of *Gaa* deficient mice have recently emerged as important determinants of the disease phenotype, drawing attention to PD neuropathology [25,59]. To understand if spinal cord defects contributed to the early and severe respiratory phenotype observed in Gaa KO^{DBA} mice (Fig. 1e, Table S1), we performed a transcriptome analysis by RNA-seq. Whole spinal cords from 4-month-old mice (Fig. 3a and b, Fig. S7a) were analysed to precisely parallel RNA expression data obtained from muscle (Fig. 2d and e). Principal component analysis (PCA) of the derived expression profiles demonstrated distinct clustering of quadriceps and spinal cord samples (Fig. S7a). In agreement with the observed clustering pattern, pairwise comparisons of spinal cord samples from both mouse lines (Gaa KO^{DBA} vs. Gaa WT^{DBA} and Gaa KO$^{B6;129}$vs. Gaa WT$^{B6;129}$) revealed smaller collections of DEGs than those detected in skeletal muscle (Figs. 2d and 3a). In addition, in the spinal cord, the number of DEGs detected in Gaa KO^{DBA} vs. Gaa WT^{DBA} (1338 DEGs) was higher than the number detected in Gaa KO$^{B6;129}$vs. Gaa WT$^{B6;129}$ (185 DEGs, Fig. 3a). This is indicative of a more severely deregulated gene expression profile in affected mice from the DBA colony (Fig. 3a). Of the 185 DEGs found in the spinal cord of Gaa KO$^{B6;129}$, 8% was shared with age-matched Gaa KO^{DBA} mice (Fig. 3a). Canonical pathway analyses with IPA on the collections of DEGs, suggested that the top shared enriched pathways, such as the neuroinflammation signalling pathway, were more active in Gaa KO^{DBA} than Gaa KO$^{B6;129}$, relative to the corresponding WT counterparts, at 4 months of age (Fig. 3b). Several other pathways were uniquely enriched in Gaa KO^{DBA} at 4 months (Fig. 3b). To further characterize the severe alterations of the spinal cord transcriptome observed in Gaa KO^{DBA} mice at 4 months, we expanded our analysis by incorporating data from public repositories. In particular, we applied the same RNA-seq data processing, differential expression testing strategies, and subsequent functional enrichment analysis with IPA, to data available from GEO entry GSE82081, which describes transcriptome profiles for the spinal cord of 6- and 16-month-old Gaa WT and Gaa KO mice, from an independent Gaa$^{B6;129}$ colony [60] (Fig. 3b). A comparison of the collections of enriched canonical pathways indicated substantial differences between young and old Gaa KO$^{B6;129}$ (4 and 6 months vs. 16 months) (Fig. 3b). Notably, the enriched pathway profile associated to spinal cord DEGs detected in contrast Gaa KO^{DBA} vs. Gaa WT^{DBA} at 4 months was similar to that observed for contrast Gaa KO$^{B6;129}$ vs. Gaa WT$^{B6;129}$ at 16-months (Fig. 3b). These data therefore suggest that Gaa KO^{DBA} mice present anticipated aberrant gene expression changes in the spinal cord compared to Gaa KO$^{B6;129}$ mice (Fig. 3a and b). Alterations of gene expression included significant activation of biological processes involved in neuroinflammation and immunity, among others (Fig. 3b). To assess the contribution of the different cell types to the transcriptomic changes we had observed in the spinal cord of Gaa KO^{DBA} relative to Gaa KO$^{B6;129}$ at 4 months, we performed a cell-type enrichment analysis using CTen (Fig. S7b). Highly significant enrichment scores were obtained for microglial and several macrophage cell populations, for both Gaa KO^{DBA} and Gaa KO$^{B6;129}$ spinal cords, with enrichment scores [-log10 (Benjamini-Hochberg p-value)] higher than 40 in all cases, suggesting the important contribution of these cell types to the spinal cord disease (Fig. S7b). The significant activation of the microglia/macrophage compartment in Gaa KO^{DBA} mice revealed by the RNA-seq at 4 months included the upregulation of known markers such as the Allograft inflammatory factor 1 (Aif1), also known as ionized calcium-binding adapter molecule 1 (Iba1), (with approximatively a 2 fold gene expression increase relative to Gaa WT^{DBA}, BH adjusted p-value=0.006), the phagocytic marker triggering receptor expressed on myeloid cells 2 (Trem2, 2 fold increase relative to Gaa WT^{DBA}, BH adjusted p-value < 0.0001) and Cluster of Differentiation 68 (CD68, 2 fold increase relative to Gaa WT^{DBA}, BH adjusted p-value = 0.004) among others (Fig S8). Significant upregulation of microglial-derived lysosomal cathepsins (Cts) and cystatin F (Cst7) was also common to the spinal cord of both Gaa KO^{DBA} and Gaa KO$^{B6;129}$, as compared to their respective WT control mice (Fig. S8). Interestingly, specific defects of the Gaa KO^{DBA} spinal cord transcriptome consisted in the significant downregulation of gene involved in synaptic transmission signalling such as serotonergic (5-HTR) and glutamatergic (GluR) receptors and the upregulation of pathways associated with neuronal cell death and pathological demyelination/remyelination processes. Activation of pro-apoptotic caspases, such as Caspase 12 (Casp12), was also found only in Gaa KO^{DBA} but not Gaa KO$^{B6;129}$ (2.6 fold increase in Gaa KO^{DBA} relative to Gaa WT^{DBA}, BH adjusted p-value < 0.0003). These pathological changes may potentially model defects in diaphragm stimulation and white matter abnormalities observed in infantile PD subjects [59,61]. Histological analysis of the cervical Gaa^{DBA} and Gaa$^{B6;129}$ spinal cord at 4 months also showed a more important loss of Choline acetyltransferase positive (Chat+) motor neurons (MN) in affected mice from the Gaa^{DBA} colony vs. Gaa KO$^{B6;129}$ mice (Fig. 3c and d). Astrogliosis, another well-known disease biomarker in the cervical Gaa KO spinal cord was instead similarly induced in Gaa KO^{DBA} and Gaa KO$^{B6;129}$ mice, as reflected by the expression of the glial fibrillary acidic protein (GFAP) by RNA-seq (approximatively 2. fold expression increases in Gaa KO relative to Gaa WT mice, BH adjusted p-value < 0.0001) and immunofluorescence analyses (Fig. S9). PAS staining of the cervical spinal cord clearly showed glycogen accumulation in Gaa-deficient motor neurons, which may include phrenic motor neurons (Fig. 3e), whose axonal projections converge into phrenic nerves and innervate the diaphragm. Overall, these findings show anticipated PD manifestations in the spinal cord of Gaa KO^{DBA} mice, and indicate that pathways involved in this process are mainly related to increased neuroinflammation, cell death and activation of immunity.

one DEG set. Asterisks denote not-significant enrichments. The colour scale represents the predicted activation state of the pathways; positive z-score values indicate higher activity in KO samples. Left column, Gaa KO^{DBA} vs. Gaa WT^{DBA}; right column, Gaa KO$^{B6;129}$ vs. Gaa WT$^{B6;129}$. (f) Comparison of log fold change (logFC) values for genes associated to fibrosis, inflammatory response, muscle regeneration and necrosis, identified in KO vs. WT contrasts in Gaa^{DBA} and Gaa$^{B6;129}$ mice. Only DEGs, with BH adjusted p-value < 0.05 and abs (logFC) > 0.5 in at least one of the two contrasts, were included in the heatmaps (number depicted in brackets). Positive and negative logFC values (red and blue colours) indicate higher expression in Gaa KO or WT, respectively.

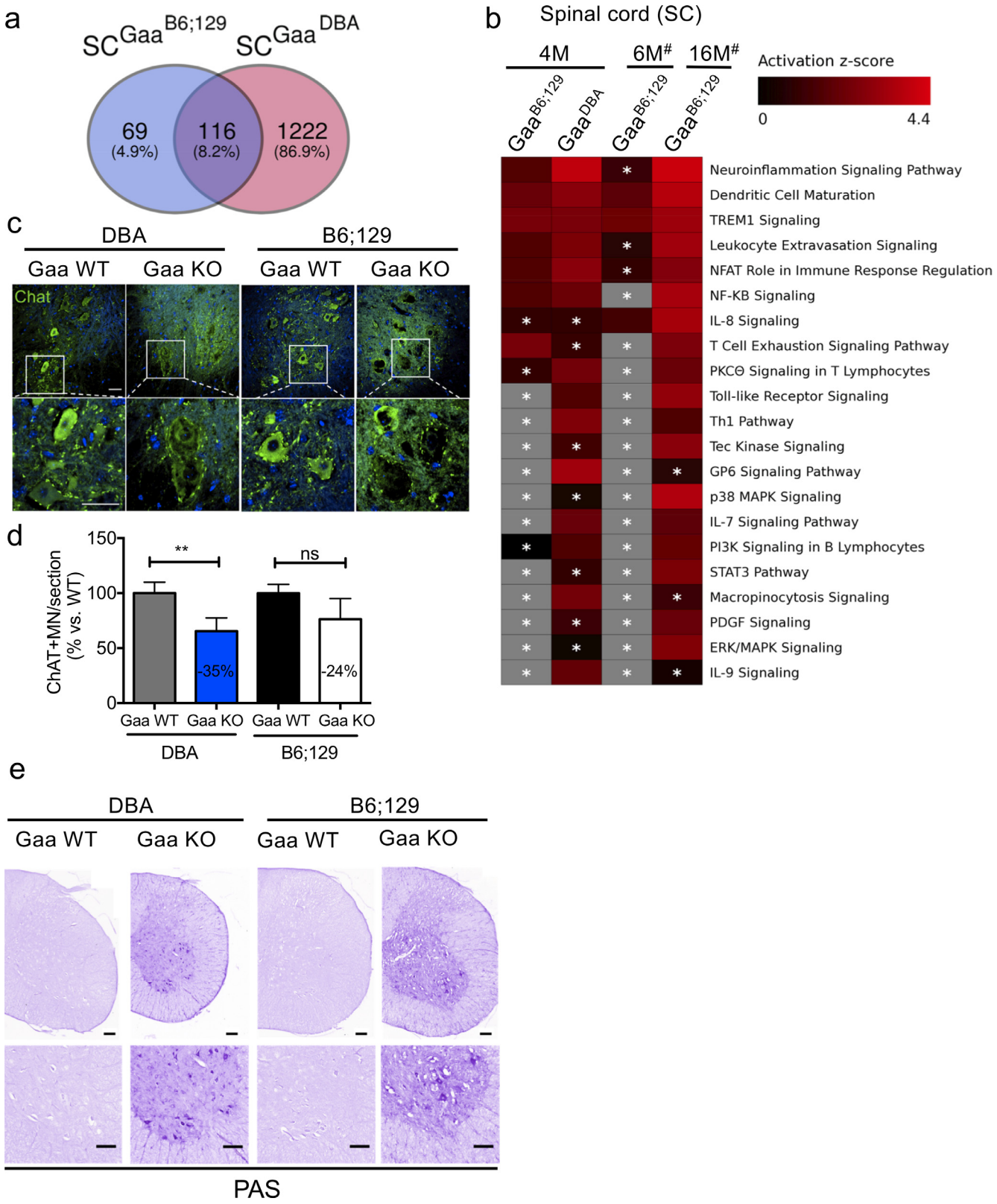

Fig. 3. Gaa KO^{DBA} mice show profound gene expression changes and motor neuron loss in spinal cord.(a-b) Downstream analysis of RNA sequencing (RNA-seq) data obtained from the entire spinal cord (SC) of 4-month-old male Gaa^{DBA} and Gaa$^{B6;129}$ mice. Expression data from genes with at least 1 count per million (CPM), in at least three samples, was used to evaluate differential expression in pairwise comparisons Gaa KO^{DBA} vs. Gaa WT^{DBA} and Gaa KO$^{B6;129}$ vs. Gaa WT$^{B6;129}$; $n = 3$ mice/sample. (a) Venn diagram distribution of specific and shared DEGs, with Benjamini-Hochberg (BH) adjusted p-value < 0.05, in each of the comparisons. (b) Comparative view of Canonical Pathway analysis results obtained with Ingenuity Pathway Analysis (IPA) for each DEG collection. The heatmap shows a selection of pathways detected as significantly enriched (p-value < 0.05) in at least one DEG set. Asterisks denote not significant enrichments. The colour scale represents the predicted activation state of the pathways; positive z-score values indicate higher activity in KO samples. The first and second columns present results for contrasts Gaa KO$^{B6;129}$ vs. Gaa WT$^{B6;129}$ and Gaa KO^{DBA} vs. Gaa WT^{DBA}, respectively, performed as part of the current study using 4-month-old mice (4M). The third and fourth columns present results for contrast Gaa KO$^{B6;129}$ vs. Gaa WT$^{B6;129}$ performed using microarray data from 6- and 16-month-old Gaa$^{B6;129}$ mice, respectively, generated by Turner et. al. (GEO entry GSE82081) [60], which were re-analysed as part of the current study. (c-d) Analyses of Choline

3.4. Gene transfer with secretable GAA rescues biochemical and transcriptome defects in neonate Gaa KO^{DBA} mice

Next, we asked whether the restoration of the missing GAA activity by AAV gene therapy was able to correct the gene expression defects observed in the skeletal muscle and spinal cord of Gaa KO^{DBA} mice. To this aim, we used AAV9 vectors encoding for a secretable version of the GAA enzyme (AAV-secGAA) [21] under the control of our previously characterized liver-muscle promoter (LiMP, ApoE-hAAT-spC5.12 in tandem) which results in long-term GAA restoration in muscle and nervous tissue upon neonatal vector delivery [47]. Since profound transcriptomic changes were observed in affected Gaa^{DBA} mice at 4 months of age, we administered AAV-secGAA vectors to neonate Gaa KO^{DBA} mice and analysed them 4 months later (Fig. 4a). Untreated Gaa KO^{DBA} and Gaa WT^{DBA} littermates were used as controls (Fig. 4a). Four months after vector administration, we found significant restoration of GAA activity (Fig. 4b) and normalisation of glycogen storage (Fig. 4c, Fig. S10a) in the skeletal muscle of Gaa KO^{DBA} mice compared to controls. AAV-mediated restoration of lysosomal GAA in the Gaa KO^{DBA} skeletal muscle also resulted in the normalisation of mitophagy and autophagy block as reflected by Parkin and p62 content (Fig. 4d–g). To evaluate the rescue of the transcriptome signature after AAV-secGAA gene therapy, we averaged the expression values from untreated Gaa KO^{DBA}, Gaa WT^{DBA} and AAV-treated Gaa KO^{DBA}, for the collection of DEGs identified in the comparison untreated Gaa KO^{DBA} vs. Gaa WT^{DBA}, and grouped the genes into clusters, using K-mean. Clusters with complementary profiles were grouped into three metaclusters containing genes with different degrees of restored expression towards wild type levels (measured in Gaa WT^{DBA}), which are referred to as “fully rescued”, “partially rescued”, and “not rescued” (Fig. 4h). Notably, the expression of ~90% of the DEGs found in the skeletal muscle of untreated Gaa KO^{DBA} mice was either fully (65.7%) or partially (24.8%) normalized by AAV-secGAA (Fig. 4h). Only a minority of disease-associated DEGs (9.5%) did not show a significant trend towards correction after AAV treatment (not rescued, Fig. 4h). Functional enrichment analysis with IPA indicated that metaclusters containing genes with fully rescued expression levels were associated to pathways involved in multiple cellular processes such as bioenergetics and metabolism (e.g. glycogen degradation, mTOR and AMPK signalling, oxidative stress, mitochondrial dysfunction), neuroinflammation, immunity, apoptosis and autophagy, among others (Fig. 4i).

Restoration of lysosomal GAA (Fig. 5a–c) and glycogen clearance (Fig. 5d) was also observed in the spinal cord of AAV-treated Gaa KO^{DBA}. Similar to what we observed in previous studies [47], the sensitivity of the GAA activity assay in the CNS was lower compared to the detection of the GAA transgene protein product by Western blot with a human-GAA-specific antibody (Fig. 5a–c). Spinal cord gene expression was either partially or fully normalised for approximately 62.5% of the identified disease-associated DEGs (Fig. 5e). The expression of 37.5% of the DEGs identified in Gaa KO^{DBA} vs. Gaa WT^{DBA} did not show a significant trend towards correction at the time of analysis (not rescued, Fig. 5e). Since neuroinflammation was found to be significantly activated in Gaa KO^{DBA} (Fig. 3b), we also focused on the DEGs associated with this pathway and found that the expression of 63.7% of them was corrected by AAV-secGAA therapy (Fig. 5f; 24% fully rescued, dark green lines; 36.4% partially rescue, light green lines; 36.4% not rescued, orange lines). Functional enrichment analysis with IPA indicated that metaclusters containing genes with fully rescued expression levels were associated to multiple pathways mainly involved in nervous system disease, neuroinflammation and immunity, in addition to energy sensing (AMPK signalling pathway) (Fig. 5g).

Overall, these results show that the efficient restoration of lysosomal GAA activity in skeletal muscle and spinal cord of Gaa KO^{DBA} mice by gene transfer with AAV-secGAA results in significantly rescue of both biochemical and transcriptome defects.

3.5. Gene transfer with secretable GAA improves muscle and respiratory phenotype in adult symptomatic Gaa KO^{DBA} mice

Based on the significant rescue observed after treatment of affected mice early after birth, we next tested if gene transfer with AAV-secGAA could also improve the disease phenotype of Gaa KO^{DBA} mice with established muscle and respiratory disease. To this aim, we used AAV9 vectors expressing secretable GAA (AAV-secGAA) under the control of a previously characterized liver-neuron promoter (LiNeuP: ApoE-hAAT-hSYN in tandem), which results in efficient hepatic and CNS co-expression of GAA upon intravenous vector delivery to adult mice [47]. The LiNeuP was chosen to achieve gene expression in the liver and at the same time rapid expression of the therapeutic GAA enzyme in the nervous tissue, to provide both a systemic (via the circulation) and local supply of GAA to the affected tissues. In this study, AAV-secGAA vectors were administered to 2-month-old Gaa KO^{DBA} mice, and the analyses were performed 3 months after gene transfer (5 months of age, Fig. 6a) to ensure enough time for the secGAA transgene to reach plateau levels in the circulation, as established in our previous studies [21], and to limit the loss of untreated Gaa KO^{DBA} due to premature death (Fig. 1b). Untreated Gaa KO^{DBA} and Gaa WT^{DBA} littermates were used as controls (Fig. 6a). At the end of the study, survival was 100% for Gaa WT^{DBA}, 60% for untreated Gaa KO^{DBA} and 80% for AAV-treated Gaa KO^{DBA}. Clear restoration of lysosomal GAA protein (Fig. 6b and c) and normalization of glycogen storage (Figs. 6d and S10b) was found in the heart, diaphragm, quadriceps and triceps of Gaa KO^{DBA} compared to untreated controls. AAV-mediated restoration of lysosomal GAA in the Gaa KO^{DBA} skeletal muscle was also associated with normalisation of muscle strength (Fig. 6e). Restoration of lysosomal GAA (Fig. 7a–e) and glycogen clearance (Fig. 7f) was also observed in the spinal cord and brain of Gaa KO^{DBA} compared to controls (Fig. 7a–f). Despite vector delivery being performed at a time of established respiratory impairment, a significant amelioration of several parameters such as Te, EF50, RT, f, EEP was measured by whole body plethysmography (Fig. 7g).

These results show that the efficient AAV-mediated restoration of GAA in muscle and nervous tissue of Gaa KO^{DBA} mice with established muscle and respiratory defects provides significant therapeutic benefit.

4. Discussion

Here we report the generation and characterization of a novel *Gaa* knock-out (KO) model, the Gaa KO^{DBA} mouse, homozygous for the *Ltbp4*$^{\Delta 36}$ allele in a mixed C57BL/6;129;DBA2/J background. In particular, male Gaa KO^{DBA} mice recapitulate the main key manifestations of PD including premature death, cardiac hypertrophy, muscle weakness, locomotor impairment, and clear respiratory defects during quiet breathing. A possible explanation of the early lethality observed in the male Gaa KO^{DBA} mouse colony could be the marked respiratory phenotype, which is specific to these animals compared to Gaa KO$^{B6;129}$ colony, combined with the muscle impairment that is similar across the two colonies. The respiratory phenotype is particularly

acetyltransferase-positive (Chat+) motor neurons (MN) in the cervical spinal cord of 4-month-old male Gaa^{DBA} and Gaa$^{B6;129}$ mice: Gaa KO^{DBA} n = 4, Gaa WT^{DBA}, Gaa WT$^{B6;129}$ and Gaa KO$^{B6;129}$ n = 3 mice/sample. The scale bar is 200 μm (top panels and bottom panels). (d) Data are depicted as average±SD, Statistical analysis: Student's t-test; $^{**}p < 0.01$. (e) Periodic acid-Schiff (PAS) staining of the cervical spinal cord (regions C3-C6), the scale bar is 200 μm (top and bottom panels). The inset shows motor neurons in the ventral horn of the cerival spinal cord grey matter.

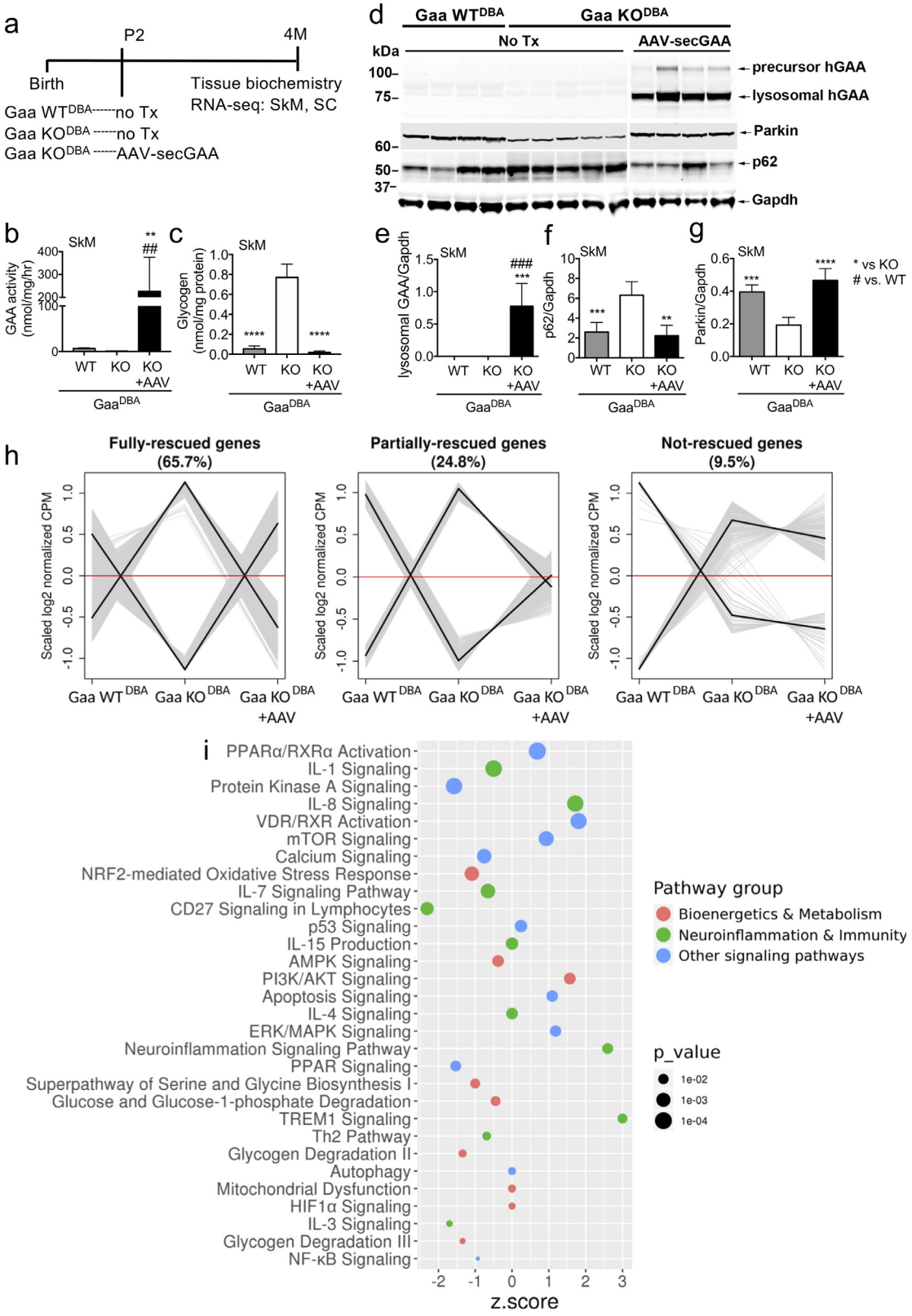

Fig. 4. Gene therapy with AAV vectors encoding for a secretable GAA variant rapidly rescues skeletal muscle defects in Gaa KO^{DBA} mice.(a) Study diagram: Gaa KO^{DBA} mice were treated by intravenous injection of AAV9 vectors encoding for a codon-optimized secretable human GAA (secGAA) under the control of the tandem liver-muscle LiMP promoter (AAV-secGAA, dose: 4×10^{10} vg/mouse, ~2×10^{13} vg/kg); littermate untreated (no Tx) Gaa KO^{DBA} and Gaa WT^{DBA} were used as controls. Vectors were delivered at postnatal day 2 (P2), analyses were performed 4 months (4M) later; SkM (skeletal muscle), SC (spinal cord). Biochemical (b-g) and downstream analysis of RNA sequencing (RNA-seq) data (h-i) of skeletal muscle (SkM) at the end of the study. (b) Analyses of GAA enzyme activity in triceps muscle. (c) Analyses of glycogen storage in triceps muscle. (d) Western blot analyses of triceps lysates with anti-human GAA, anti-Parkin, and anti-p62 antibodies, anti-Gapdh antibody was used as loading control. The molecular weight marker (kDa) is depicted. The lanes were run on the same gel but were non-contiguous. Western blot quantification is shown in panels e (GAA), f (p62) and g (Parkin). (b-g) Gaa WT^{DBA} ($n = 4$), Gaa KO^{DBA} ($n = 5$), Gaa KO^{DBA} +AAV ($n = 4$). Data are depicted as average±SD. (h) Gene expression clusters. Expression profiles for 2573 DEGs with abs (logFC) > 0.5, detected in contrast untreated Gaa KO^{DBA} vs. Gaa WT^{DBA}, were constructed by recovering averaged expression values from untreated Gaa KO^{DBA}, Gaa WT^{DBA} and AAV-treated Gaa KO^{DBA} samples, and assigned to

relevant to PD, since currently available *Gaa* KO mice present very mild respiratory defects [18, 21–27]. Respiratory problems instead manifest in all forms of the disease, representing one of the leading causes of morbidity, in addition to IOPD-specific cardiomyopathy [5, 28–32]. While cardiac problems have been widely reported to be effectively treated by ERT [5], the effective treatment of the PD respiratory phenotype still represents a medical need [14, 32]. Therefore, the male *Gaa* KO^{DBA} model we presented here is a useful tool to study the pathophysiology of respiratory defects in PD and to test the efficacy of novel therapeutic strategies. Interestingly, normal survival with late-onset cardiac hypertrophy and respiratory defects were observed in female Gaa KO^{DBA}, in agreement with previous studies in male and female mdx-DBA2/J mouse models of Duchenne muscular dystrophy (DMD) [62], thus suggesting that male Gaa KO^{DBA} mice are a more stringent model of PD.

Interestingly, we found that the DBA2/J background (commonly referred to as D2), harbouring the modifier *Ltbp4*$^{\Delta 36}$ allele [42] modulates the severity of the disease phenotype in the Gaa KO mouse. A previous study by Raben et al. reported that the genetic background modulates the severity of muscle disease in Gaa KO mice [63], showing a milder muscle phenotype in GAA KO in a mixed C57BL/6;129; FVB background compared to the most severe Gaa KO$^{B6;129}$ strain [63]. Notably, here we report for the first time that the genetic background also modulates the severity of respiratory defects and neuropathology in Gaa KO mice.

By comparing side-by-side the disease phenotype of the Gaa KO$^{B6;129}$ mouse, the most used and severe PD model, to our newly generated Gaa KO^{DBA} mouse, we observed similar muscle disease while more pronounced neuropathology and respiratory defects in the Gaa KO^{DBA} mouse. Muscle strength and ultrastructure were found to be similarly affected in Gaa KO$^{B6;129}$ and Gaa KO^{DBA}. While the disease phenotype of Gaa KO^{DBA} mice in the C57BL/6;129;DBA2/J background showed low variability, future work will be aimed at obtaining a mouse colony fully backcrossed into DBA2/J to perform additional studies on the impact of the *Ltbp4*$^{\Delta 36}$ allele on PD.

In our study, in agreement with the other assessments, transcriptomic analysis by RNA sequencing showed a similar deregulation of muscle gene expression in the affected mice from both strains. Transcriptional changes in the skeletal muscle of affected Gaa^{DBA} mice were also found to be highly similar to those of affected Gaa$^{B6;129}$ upon the analysis of public gene expression datasets from the Gaa$^{B6;129}$ strain [48,58]. Both Gaa KO$^{B6;129}$ and Gaa KO^{DBA} from the present study showed a significant upregulation of cellular pathways involved in inflammation, immunity, oxidative stress and the deregulation of pathways involved in cellular energy sensing and metabolism (e.g. mTOR, AMPK). Muscle regenerative processes were also induced in affected mice, as reflected by the upregulation of fetal Myosins (*Myh 3* and *Myh8*) and *Myogenin* expression, which are recognized markers of muscle regeneration in several myopathies [64]. The upregulation of several caspases such as 1, 3, and 6 in skeletal muscle also suggests the activation of a degenerative/regenerative process, as reported in other forms of muscular dystrophy [65]. Recent studies reported that in PD mice the upregulation of genes associated with muscle regeneration is accompanied to a low number of regenerating myofibers due to reduced activation of muscle satellite cells [66]. Interestingly, in the present study transcriptomic analyses of Gaa KO skeletal muscle showed an important downregulation of *Klotho*, whose deficiency has been linked to impaired muscle regeneration due to defects in muscle progenitor cells [67]. Our findings therefore shed light on novel mechanisms contributing to the impairment of muscle regeneration in PD. Consistent with our observations, previous reports in mouse models of muscular dystrophy (MD), such as the Dystrophin-deficient mdx mice, have shown that the DBA2/J background does not worsen muscle grip strength and the induction of regeneration-associated Myh3 and Myh8, when compared to the parental background [68]. In mdx mice, the DBA2/J background also exacerbates muscle inflammation, permeability and fibrosis, which are all prominent features of MD in mdx-C57BL/10 (and other MD strains), and are caused by the defects of dystrophin glycoprotein complex (DGC) at the sarcolemma [68]. Here, we observed that the increased activation of inflammation-associated genes and the deregulation of genes associated with fibrosis and necrosis was similar in the muscle of Gaa KO^{DBA} compared to Gaa KO$^{B6;129}$. The deregulation of these pathways, however, was not associated with muscle histopathological defects (e.g. muscle scars, fibrosis and infiltration of mononuclear cells) in any muscle analysed, including the diaphragm, which is particularly relevant to the respiratory function. This difference between MD and PD models may be explained by the different nature, function and pathological consequences of *Gaa* deficiency, which results in a mostly preserved muscle fibre structure. Dystrophin deficiency and other DGC defects instead result in the disruption of the muscle sarcolemma, muscle necrosis, important infiltration of immune cells, and consequent deposition of fibrotic tissue and calcifications [68]. Of note, our previous analyses in Gaa KO$^{B6;129}$ at late stages of the disease (18 months) also failed to reveal skeletal muscle fibrosis and inflammatory infiltrates, despite the inductions of fibrotic and inflammatory gene expression [48]. Clinical studies in muscle of IOPD subjects also showed that, differently from MD, fibrosis and chronic immune activation are not the main features of PD muscle, despite the activation of the underlying signalling pathways [69,70].

Mildly altered respiratory function has been reported in mdx-DBA2/J despite presenting a more severely affected diaphragm compared to the mdx-C57BL/10 strain. Furthermore, TGFβ inhibitors have been reported to improve the respiratory function in mdx mice [71]. Here we found that Gaa KO^{DBA} show severe early-onset alterations of the respiratory function but no apparent worsening of the diaphragm histopathology. This suggests that increased TGFβ release in Gaa KO^{DBA} mice, which are homozygous for the *Ltbp4*$^{\Delta 36}$ allele, may have an important role in the aetiology of the observed respiratory defects. Differently from PD, the high basal level of TGFβ in the mdx muscle [71] and the superior activation of the TGFβ-SMAD2/3 signalling pathway in MD myotubes [72] may possibly synergize with the increased TGFβ release in the DBA2/J background [42] to significantly worsen MD. Notably, we also found that the early restoration of the missing enzyme in skeletal muscle of Gaa KO^{DBA} mice by systemic administration of AAV-secGAA vectors was able to normalize glycogen content, autophagy/mitophagy block and transcriptome gene expression. The expression of 90.5% of the deregulated genes identified in the Gaa KO^{DBA} skeletal muscle was indeed fully or partially corrected compared to Gaa WT^{DBA} 4 months after AAV-secGAA administration. Correction of pathological transcriptome changes was observed in multiple cell pathways including glucose/glycogen metabolism, energy sensing (mTOR and AMPK signalling), apoptosis, autophagy, inflammation (NFkB signalling) and mitochondrial function, to cite some. The rescue of aberrant mTOR and AMPK signalling

6 clusters using K-mean. Clusters with complementary expression profiles were combined to define three metaclusters, containing genes whose expression levels had been fully rescued (65.7% of DEGs), partially rescued (24.8% of DEGs) or not rescued (9.5% of DEGs) after treatment of Gaa KO^{DBA} with AAV-secGAA. Normalized expression counts, averaged for each condition and scaled for each gene, are represented on the Y-axis. Grey lines represent the expression profile of individual genes. Black lines represent average expression profiles for each of the combined clusters. (i) Functional enrichment analysis with Ingenuity Pathway Analysis (IPA) for the set of fully rescued genes. The dot plot represents Benjamini-Hochberg (BH) adjusted *p*-values and activation z-scores, for the set of 30 canonical pathways associated to significant enrichment *p*-values (BH *p*-value < 0.05). Statistical analysis: One-way ANOVA with Tukey post-hoc (b-c, e-g). Asterisks and hash marks on the bars show significant differences vs. mouse cohorts specified in the graph legends; $^{*}p < 0.05$, $^{**}p < 0.01$, $^{***}p < 0.001$, $^{****}p < 0.0001$, $\#\#p < 0.01$, $\#\#\#p < 0.001$.

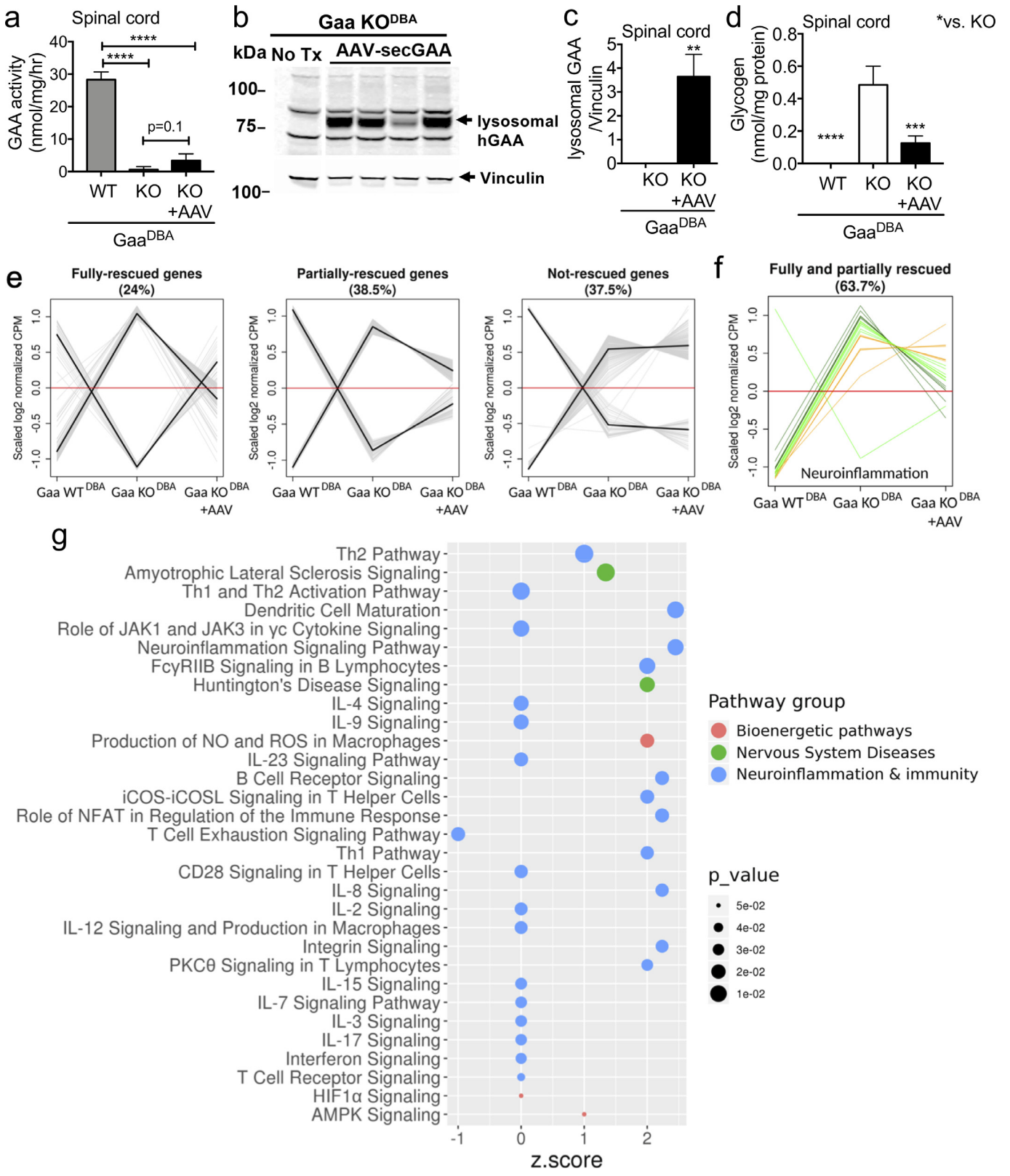

Fig. 5. Gene therapy with AAV-secGAA vectors improves the spinal cord disease phenotype in Gaa KO^{DBA} mice.(a-g) Gaa KO^{DBA} mice were treated by intravenous injection of AAV9 vectors encoding for a codon-optimized secretable human GAA (secGAA) under the control of the tandem liver-muscle LiMP promoter (AAV-secGAA, dose: 4×10^{10} vg/mouse, ~2×10^{13} vg/kg); littermate untreated (no Tx) Gaa KO^{DBA} and Gaa WT^{DBA} were used as controls. Vector was delivered at postnatal day 2, analyses were performed 4 months later (study diagram in Figure 4a). Biochemical (a-d) and downstream analysis of RNA sequencing (RNA-seq) data (e-g) in spinal cord samples at the end of the study are shown. (a) Analyses of GAA enzyme activity in the spinal cord. (b-c) Western blot analyses of spinal cord lysates with anti-human GAA antibody, anti-Vinculin antibody was used as loading control. The molecular weight marker (kDa) is depicted. The lanes were run on the same gel but were non-contiguous. Western blot quantification is shown in panel c. (d) Analyses of glycogen storage in the spinal cord. (a-d) Gaa WT^{DBA} ($n = 4$), Gaa KO^{DBA} ($n = 5$), Gaa KO^{DBA} +AAV ($n = 4$). Data are depicted as average±SD. (e) Gene expression clusters. Expression profiles for 137 DEGs with abs (logFC) > 0.5, detected in contrast untreated Gaa KO^{DBA} vs. Gaa WT^{DBA}, were constructed by recovering averaged expression values from untreated Gaa KO^{DBA}, Gaa WT^{DBA} and AAV-treated Gaa KO^{DBA} samples, and assigned to 6 clusters using K-mean. Clusters with complementary expression profiles were combined to define three

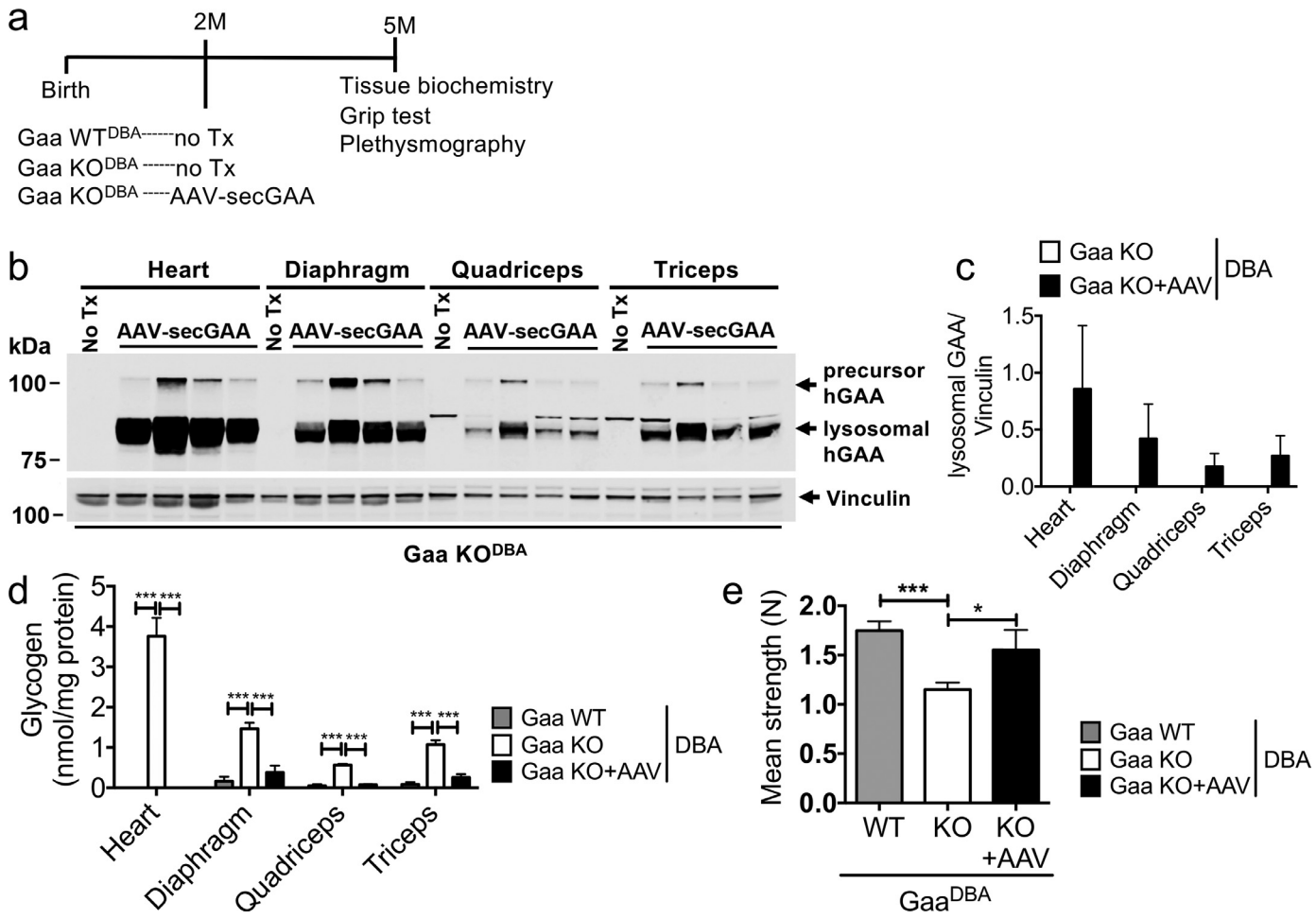

Fig. 6. AAV-secGAA gene transfer rescues glycogen accumulation and muscle strength in adult Gaa KO^{DBA} mice with established disease.(a) Study diagram: Gaa KO^{DBA} mice (n = 5) were treated by intravenous injection of AAV9 vectors encoding for a codon-optimized secretable human GAA (secGAA) under the control of the tandem liver-neuron LiNeuP promoter (AAV-secGAA, dose: 2×10^{12} vg/kg); littermate untreated (no Tx) Gaa KO^{DBA} (n = 5) and Gaa WT^{DBA} (n = 5) were used as controls. Vectors were delivered to 2-month-old mice (2M), analyses were performed 3 months later in 5-month-old mice (5M). (b-c) Western blot analyses of heart, diaphragm, quadriceps and triceps muscle lysates with anti-human GAA antibody, anti-Vinculin antibody was used as loading control. The molecular weight marker (kDa) is depicted. Western blot quantification is shown in panel c. (d) Analyses of glycogen storage in of heart, diaphragm, quadriceps and triceps muscles. (e) Muscle strength measured by 4-limb grip strength test. (b-e) The number of alive mice at the end of the study was: Gaa WT^{DBA} (n = 5), Gaa KO^{DBA} (n = 3), Gaa KO^{DBA} +AAV (n = 4). Data are depicted as average±SD. Statistical analysis: Multiple t-test with Holm-Sidak post-hoc (c), Two-way ANOVA with Tukey post-hoc (d), One-way ANOVA with Tukey post-hoc (e);$^{*}p < 0.05$, $^{**}p < 0.01$, $^{***}p < 0.001$.

is particularly relevant, since these pathways have been reported to be difficult to correct by ERT in Gaa KO mice [73,74].

Different from muscle, transcriptomic analyses of the Gaa KO^{DBA} spinal cord showed more profound changes as compared to age-matched Gaa KO$^{B6;129}$. The number of significantly deregulated genes was indeed ~7 times higher in the Gaa KO^{DBA} spinal cord than Gaa KO$^{B6;129}$ at 4 months of age. Microarray analyses of the mid-cervical spinal cord from 6- and 16-month old Gaa KO$^{B6;129}$ mice, previously reported by Turner et al., showed that the number of deregulated genes increases with age, possibly reflecting disease severity and progression [60]. Interestingly, analysing side by side our gene expression data to that generated by Turner el al. [60], we found that the disease-associated gene function signature in the spinal cord of 4-moth-old Gaa KO^{DBA} was similar to that of 16-month-old Gaa KO$^{B6;129}$ mice. This finding suggests that Gaa KO^{DBA} mice present with an anticipated disease phenotype affecting the spinal cord. Our RNA-seq analyses also showed that the transcriptomic signature of the Gaa KO^{DBA} spinal cord was characterized by the important upregulation of neuroinflammation and contribution of the microglia/macrophage compartment. A similar transcriptomic signature has been observed in the nervous tissue of other mouse models of lysosomal storage disease (LSD) with a prominent neurologic disease phenotype [75,76]. Notably, RNA-seq of the Gaa KO^{DBA} spinal cord also revealed a significant upregulation of genes associated with neuronal cell death and pathological demyelination/remyelination processes. Consistent with the unique caspase upregulation we found in Gaa KO^{DBA} spinal cord by RNA-seq, a more important loss of motor neurons was also found in these mice compared to age-matched Gaa KO$^{B6;129}$ at 4-months by histological analyses. Glycogen storage was also prominent in putative motor neurons in cervical spinal regions

metaclusters, containing genes whose expression levels had been fully rescued (24% of DEGs), partially rescued (38.5% of DEGs) or not rescued (37.5 % of DEGs) after treatment of Gaa KO^{DBA} with AAV-secGAA. Normalized expression counts, averaged for each condition and scaled for each gene, are represented on the Y-axis. Grey lines represent the expression profile of individual genes. Black lines represent average expression profiles for each of the combined clusters. (f) Combined representation of the three metaclusters depicted in panel e, filtered to describe exclusively genes involved in neuroinflammation: fully rescued, dark green lines; partially rescued, light green lines; not rescued, orange lines. (g) Functional enrichment analysis with Ingenuity Pathway Analysis (IPA) for the set of fully rescued genes. The dot plot represents Benjamini-Hochberg (BH) adjusted p-values and activation z-scores, for the set of 31 canonical pathways associated to significant enrichment p-values (BH p-value < 0.05). (c-d) Asterisks on the bars show significant differences vs. mouse cohorts specified in the graph legends; $^{*}p < 0.05$, $^{**}p < 0.01$, $^{***}p < 0.001$, $^{****}p < 0.0001$.

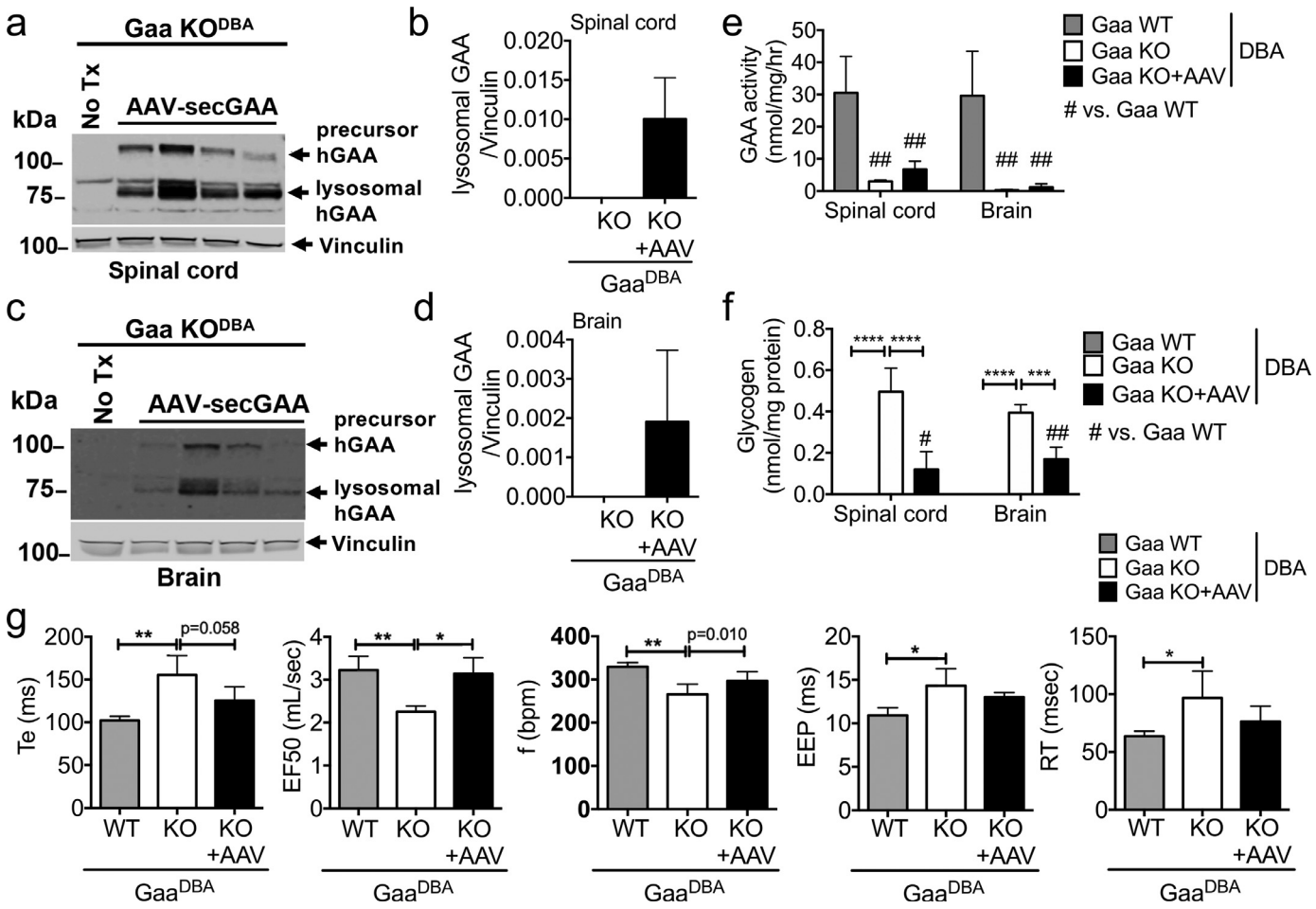

Fig. 7. AAV-secGAA gene transfer rescues glycogen accumulation in the spinal cord and improves respiratory function in adult Gaa KO^{DBA} mice with established disease.(a-g) Gaa KO^{DBA} mice (n = 5) were treated by intravenous injection of AAV9 vectors encoding for a codon-optimized secretable human GAA (secGAA) under the control of the tandem liver-neuron LiNeuP promoter (AAV-secGAA, dose: 2×10^{12} vg/kg); littermate untreated (no Tx) Gaa KO^{DBA} (n = 5) and Gaa WT^{DBA} (n = 5) were used as controls. Vector was delivered to 2-month-old mice (2M), analyses were performed 3 months later in 5-month-old mice (study diagram in Figure 6a). (a-d) Western blot analyses of spinal cord (a-b) and brain (c-d) lysates with anti-human GAA antibody, anti-Vinculin antibody was used as loading control. The molecular weight marker (kDa) is depicted. Western blot quantification is shown in panels b and d. (e) Analyses of GAA enzyme activity in spinal cord and brain. (f) Analyses of glycogen storage in in spinal cord and brain. (g) Analyses of respiratory function measured by whole body plethysmography during quiet breathing: expiratory time (Te), mid expiratory flow (EF50), frequency of breathing (f), end expiratory pause (EEP), retention time (RT). (a-g) The number of alive mice at the end of the study was: Gaa WT^{DBA} (n = 5), Gaa KO^{DBA} (n = 3), Gaa KO^{DBA} +AAV (n = 4). Data are depicted as average±SD. Statistical analysis: Student's t-test (b, d); Two-way ANOVA with Tukey post-hoc (e, f); One-way ANOVA with Tukey post-hoc (g). Asterisks and hash marks on the bars show significant differences vs. mouse cohorts specified in the graph legends; $^{*}p < 0.05$, $^{**}p < 0.01$, $^{***}p < 0.001$, $^{****}p < 0.001$, $\#p < 0.05$, $\#\#p < 0.01$.

containing the phrenic motor neurons, which controls the respiratory diaphragm. The activation of the cathepsin/cystatin axis we observed in Gaa KO mice also reveals novel neuropathologic mechanisms which may be important to further characterize since the deregulation of these genes has been related to pathological demyelination/remyelination processes and neuronal cell death in models of amyotrophic lateral sclerosis (ALS) [77] and other LSDs [78]. Notably, white matter hypersensitive foci and demyelination have been observed in IOPD and LOPD [59].

As observed in muscle, we showed that the systemic early administration of AAV-secGAA vectors to Gaa KO^{DBA} mice restored lysosomal GAA and cleared pathological glycogen storage in the spinal cord. At only 4 months after AAV-secGAA administration, the expression of about 63% of the DEGs in the spinal cord of Gaa KO^{DBA} was fully or partially corrected compared to Gaa WT^{DBA}. The rescue of pathological transcriptome changes in the spinal cord of PD mice is an unprecedented observation that has important implications for PD treatment. We have previously reported that the clearance of pathological glycogen accumulation in the nervous system of PD mice is a time-dependent process, therefore long-term follow-up after AAV gene therapy is required to properly evaluate the effect of GAA restoration in this tissue [21]. In the present study, the expression of a large proportion of the deregulated genes found in the Gaa KO^{DBA} spinal cord was restored to wild type levels at an early time point after neonatal administration of AAV-secGAA vectors. These findings represent the first evidence that profound transcriptomic defects occurring in the nervous system of *Gaa*-deficient mice can be rapidly improved by restoring the missing enzyme activity. The rescue of disease-associated transcriptome changes in the Gaa KO^{DBA} spinal cord included a significant decrease of neuroinflammation and immune activation, and the correction of disease-related signalling pathways (e.g. ALS and Huntington disease signalling), among others.

ERT has been widely reported to effectively correct cardiomyopathy in IOPD, slightly improve or stabilize muscle function in LOPD while providing modest effects on the respiratory problems, likely due to limited targeting of the CNS [5,14,32–37,41]. We have previously reported that liver AAV gene therapy using a secretable human GAA results in a dose- and time-dependent restoration of lysosomal GAA in the CNS of Gaa KO$^{B6;129}$ mice [21]. A faster restoration of lysosomal GAA in the nervous system can be achieved combining co-expression of secretable GAA in both liver and neurons using a tandem liver-neuron promoter (LiNeuP) [47]. In the present study, we used this latter approach and showed for the first time that it allows

to improve at the same time muscle strength and respiratory defects after vector administration to mice with already established defects. Treatment of PD by *GAA* gene transfer has intuitively higher therapeutic potential at early disease stages, however our findings suggest that phenotype improvement can be achieved by restoring therapeutic levels of enzyme activity even in a time of fully manifested dysfunctions of muscle and nervous system. Future studies will tell whether early restoration of GAA activity in the nervous tissue is needed to prevent irreversible disease manifestations linked to neuronal cell death.

Seminal studies suggested that neuronal deficit contributes to respiratory defects in mice and PD subjects [25,79]. Consistently, the present study provides compelling evidence that profound transcriptomic changes in the spinal cord are accompanied with severe respiratory defects, as we observed in Gaa KO^{DBA} mice, but not Gaa $KO^{B6;129}$ mice. Our findings thus show that in *Gaa* deficient mice the spinal cord disease plays a key role in the aetiology of respiratory impairment in PD, and that the genetic background, including the *Ltbp4* haplotype, impacts upon its onset and severity. The pronounced neuroinflammation observed in the spinal cord of Gaa KO^{DBA} mice may be the underlying cause of the severe motor neuron loss and respiratory dysfunction in these animals. This, would be a direct effect of the increased release of TGFβ associated with the DBA2/J background, or other modifiers in addition to the $Ltbp4^{\Delta 36}$ alleles. Future work will be aimed at dissecting the causative molecular mechanism underlying the early-onset spinal cord and respiratory phenotype of Gaa KO^{DBA} mice. The identification of modifier genes in PD severity and response to ERT still represents an important challenge in the field [12]. Despite the current study being limited to a mouse model, other genetic studies have shown that *LTBP4* is a modifier gene in human diseases such as DMD, allowing to predict the age of ambulatory loss [44–46]. Therefore, based on our findings, it could be of interest to evaluate the impact of *LTBP4* as modifier gene in PD subjects and its relevance as new therapeutic target. Interestingly, multiple strategies could be exploited to counteract the increased release of TGFβ from the extracellular matrix, as determined by the "detrimental" $Ltbp4^{\Delta 36}$ allele [42,71,80–83].

In conclusion, this work provides a unique, highly stringent mouse model of PD, which offers insights into mechanisms and biomarkers of PD, and demonstrates novel proof-of-concept of the efficacy of systemic AAV vector gene transfer in addressing the neuromuscular pathology in PD.

5. Contributors

P.C. and F.M. conceived the study. P.C. and F. M. wrote the manuscript. P.C. directed and performed the experiments, data analysis and the interpretation of results. U.C. and M.J.G. performed the bioinformatic analyses of RNA sequencing data. P.S. generated most of the biochemical raw data and performed mouse genotyping. L.v.W. performed animal experimentation and the delivery of AAV vectors in mice. L.v.W. and N.D. managed the animal experimentation and the collection of mouse samples. N.G. and G.T. performed plethysmography, grip test, wire hang and rotarod tests in mice. B.G. performed histological analyses. U.C, M.M.N. and J.K.L. performed electron microscopy analyses. M.G.B. and M.C. performed spinal cord histological analyses. F.C., S.C. and M.S.S. produced the AAV vector preparations. All authors read and approved the final version of the manuscript.

Data sharing statement

The RNA-seq data generated in this manuscript are available at NCBI's Gene Expression Omnibus (https://www.ncbi.nlm.nih.gov/geo) and publicly accessible through GEO Series accession number GSE156230 (https://www.ncbi.nlm.nih.gov/geo/query/acc.cgi?acc=GSE156230). Data deposition procedures in GEO ensure MIAME- and MINSEQE-compliant data submission. The nucleotide sequence of the secGAA and tandem promoters used in this manuscript are reported in our previous works [21, 47]. All other data and materials are available upon request upon signing a material transfer agreement.

Declaration of Competing Interest

P.C. and F.M. are inventors in patent applications describing the secGAA technology and concerning the treatment of Pompe disease by AAV licensed to Spark Therapeutics (F.M.: WO2018046774, WO2018046775; P.C: WO2018046775). P.C and F.M. are inventors in a patent application describing the use of tandem promoters (WO2019154939A1). F.M. is employee and equity holder of Spark Therapeutics, Inc., a Roche company. U.C. received salary from the Marie Skłodowska-Curie Actions Individual Fellowship (MSCA-IF) grant agreement no. 797144. All other authors declare no conflict of interest. This work was partially supported by Spark Therapeutics under a sponsored research agreement (to Genethon).

Acknowledgments

This work was supported by Genethon and the French Muscular Dystrophy Association (AFM, to F.M.). It was also supported by the European Union's research and innovation program under grant agreement no. 667751 (to F.M.), the European Research Council Consolidator Grant under grant agreement no. 617432 (to F.M.), Marie Skłodowska-Curie Actions Individual Fellowship (MSCA-IF) grant agreement no. 797144 (to U.C.), and by Spark Therapeutics under a sponsored research agreement. We thank Emilie Bertil-Froideveaux (Genethon) and Fanny Bordier (Genethon) and the Genethon "Histology core facility" for technical help with histology; Simon Jimenez (Genethon) and the Genethon "Imaging Core Facility" for technical help with histological image acquisition.

Supplementary materials

Supplementary material associated with this article can be found, in the online version, at doi:10.1016/j.ebiom.2020.103052.

References

[1] Kishnani PS, Steiner RD, Bali D, Berger K, Byrne BJ, Case LE, et al. Pompe disease diagnosis and management guideline. Genet Med 2006;8(5):267–88.
[2] van der Ploeg AT, Reuser AJ. Pompe's disease. Lancet 2008;372(9646):1342–53.
[3] . van Capelle CI, van der Meijden JC, van den Hout JM, Jaeken J, Baethmann M, Voit T, et al. Childhood Pompe disease: clinical spectrum and genotype in 31 patients. Orphanet J Rare Dis 2016;11(1):65.
[4] Chan J, Desai AK, Kazi ZB, Corey K, Austin S, Hobson-Webb LD, et al. The emerging phenotype of late-onset Pompe disease: a systematic literature review. Mol Genet Metab 2017;120(3):163–72.
[5] Kishnani PS, Hwu WL, Mandel H, Nicolino M, Yong F, Corzo D, et al. A retrospective, multinational, multicenter study on the natural history of infantile-onset Pompe disease. J Pediatr 2006;148(5):671–6.
[6] Kroos MA, Pomponio RJ, Hagemans ML, Keulemans JL, Phipps M, DeRiso M, et al. Broad spectrum of Pompe disease in patients with the same c.-32-13T->G haplotype. Neurology 2007;68(2):110–5.
[7] Kroos M, Hoogeveen-Westerveld M, van der Ploeg A, Reuser AJ. The genotype-phenotype correlation in Pompe disease. Am J Med Genet C Semin Med Genet 2012;160C(1):59–68.
[8] . Bergsma AJ, In 't Groen SLM, van den Dorpel JJA, van den Hout H, van der Beek N, Schoser B, et al. A genetic modifier of symptom onset in Pompe disease. EBioMedicine 2019;43:553–61.
[9] . de Filippi P, Ravaglia S, Bembi B, Costa A, Moglia A, Piccolo G, et al. The angiotensin-converting enzyme insertion/deletion polymorphism modifies the clinical outcome in patients with Pompe disease. Genet Med 2010;12(4):206–11.
[10] De Filippi P, Saeidi K, Ravaglia S, Dardis A, Angelini C, Mongini T, et al. Genotype-phenotype correlation in Pompe disease, a step forward. Orphanet J Rare Dis 2014;9:102.
[11] Baek RC, Palmer R, Pomponio RJ, Lu Y, Ma X, McVie-Wylie AJ. The influence of a polymorphism in the gene encoding angiotensin converting enzyme (ACE) on

treatment outcomes in late-onset Pompe patients receiving alglucosidase alfa. Mol Genet Metab Rep 2016;8:48–50.
[12] Kuperus E, van der Meijden JC, In 't Groen SLM, Kroos MA, Hoogeveen-Westerveld M, Rizopoulos D, et al. The ACE I/D polymorphism does not explain heterogeneity of natural course and response to enzyme replacement therapy in Pompe disease. PLoS One 2018;13(12):e0208854.
[13] Raben N, Nagaraju K, Lee E, Kessler P, Byrne B, Lee L, et al. Targeted disruption of the acid alpha-glucosidase gene in mice causes an illness with critical features of both infantile and adult human glycogen storage disease type II. J Biol Chem 1998;273(30):19086–92.
[14] Kohler L, Puertollano R, Raben N. Pompe disease: from basic science to therapy. Neurotherapeutics 2018;15(4):928–42.
[15] Sun B, Brooks ED, Koeberl DD. Preclinical development of new therapy for glycogen storage diseases. Curr Gene Ther 2015;15(4):338–47.
[16] Sidman RL, Taksir T, Fidler J, Zhao M, Dodge JC, Passini MA, et al. Temporal neuropathologic and behavioral phenotype of 6neo/6neo Pompe disease mice. J Neuropathol Exp Neurol 2008;67(8):803–18.
[17] Fukuda T, Ahearn M, Roberts A, Mattaliano RJ, Zaal K, Ralston E, et al. Autophagy and mistargeting of therapeutic enzyme in skeletal muscle in Pompe disease. Mol Ther 2006;14(6):831–9.
[18] Raben N, Hill V, Shea L, Takikita S, Baum R, Mizushima N, et al. Suppression of autophagy in skeletal muscle uncovers the accumulation of ubiquitinated proteins and their potential role in muscle damage in Pompe disease. Hum Mol Genet 2008;17(24):3897–908.
[19] Turner SM, Hoyt AK, ElMallah MK, Falk DJ, Byrne BJ, Fuller DD. Neuropathology in respiratory-related motoneurons in young Pompe (Gaa(-/-)) mice. Respir Physiol Neurobiol 2016;227:48–55.
[20] Falk DJ, Todd AG, Lee S, Soustek MS, ElMallah MK, Fuller DD, et al. Peripheral nerve and neuromuscular junction pathology in Pompe disease. Hum Mol Genet 2015;24(3):625–36.
[21] Puzzo F, Colella P, Biferi MG, Bali D, Paulk NK, Vidal P, et al. Rescue of Pompe disease in mice by AAV-mediated liver delivery of secretable acid alpha-glucosidase. Sci Transl Med 2017;9(418).
[22] Falk DJ, Soustek MS, Todd AG, Mah CS, Cloutier DA, Kelley JS, et al. Comparative impact of AAV and enzyme replacement therapy on respiratory and cardiac function in adult Pompe mice. Mol Ther Methods Clin Dev 2015;2:15007.
[23] Falk DJ, Mah CS, Soustek MS, Lee KZ, Elmallah MK, Cloutier DA, et al. Intrapleural administration of AAV9 improves neural and cardiorespiratory function in Pompe disease. Mol Ther 2013;21(9):1661–7.
[24] Mah C, Pacak CA, Cresawn KO, Deruisseau LR, Germain S, Lewis MA, et al. Physiological correction of Pompe disease by systemic delivery of adeno-associated virus serotype 1 vectors. Mol Ther 2007;15(3):501–7.
[25] DeRuisseau LR, Fuller DD, Qiu K, DeRuisseau KC, Donnelly Jr. WH, Mah C, et al. Neural deficits contribute to respiratory insufficiency in Pompe disease. Proc Natl Acad Sci USA 2009;106(23):9419–24.
[26] Mah CS, Falk DJ, Germain SA, Kelley JS, Lewis MA, Cloutier DA, et al. Gel-mediated delivery of AAV1 vectors corrects ventilatory function in Pompe mice with established disease. Mol Ther 2010;18(3):502–10.
[27] Keeler AM, Zieger M, Todeasa SH, McCall AL, Gifford JC, Birsak S, et al. Systemic delivery of AAVB1-GAA clears glycogen and prolongs survival in a mouse model of Pompe disease. Hum Gene Ther 2019;30(1):57–68.
[28] van der Beek NA, van Capelle CI, van der Velden-van Etten KI, Hop WC, van den Berg B, Reuser AJ, et al. Rate of progression and predictive factors for pulmonary outcome in children and adults with Pompe disease. Mol Genet Metab 2011;104 (1-2):129–36.
[29] . Gungor D, de Vries JM, Hop WC, Reuser AJ, van Doorn PA, van der Ploeg AT, et al. Survival and associated factors in 268 adults with Pompe disease prior to treatment with enzyme replacement therapy. Orphanet J Rare Dis 2011;6:34.
[30] Hagemans ML, Winkel LP, Hop WC, Reuser AJ, Van Doorn PA, Van der Ploeg AT. Disease severity in children and adults with Pompe disease related to age and disease duration. Neurology 2005;64(12):2139–41.
[31] Laforet P, Laloui K, Granger B, Hamroun D, Taouagh N, Hogrel JY. et al. The French Pompe registry. Baseline characteristics of a cohort of 126 patients with adult Pompe disease. Rev Neurol 2013;169(8-9):595–602.
[32] Fuller DD, ElMallah MK, Smith BK, Corti M, Lawson LA, Falk DJ, et al. The respiratory neuromuscular system in Pompe disease. Respir Physiol Neurobiol 2013;189 (2):241–9.
[33] Kishnani PS, Corzo D, Leslie ND, Gruskin D, Van der Ploeg A, Clancy JP, et al. Early treatment with alglucosidase alpha prolongs long-term survival of infants with Pompe disease. Pediatr Res 2009;66(3):329–35.
[34] van der Ploeg AT, Clemens PR, Corzo D, Escolar DM, Florence J, Groeneveld GJ, et al. A randomized study of alglucosidase alfa in late-onset Pompe's disease. N Engl J Med 2010;362(15):1396–406.
[35] Anderson LJ, Henley W, Wyatt KM, Nikolaou V, Waldek S, Hughes DA, et al. Effectiveness of enzyme replacement therapy in adults with late-onset Pompe disease: results from the NCS-LSD cohort study. J Inherit Metab Dis 2014;37(6):945–52.
[36] Schoser B, Stewart A, Kanters S, Hamed A, Jansen J, Chan K, et al. Survival and long-term outcomes in late-onset Pompe disease following alglucosidase alfa treatment: a systematic review and meta-analysis. J Neurol 2017;264(4):621–30.
[37] Papadopoulos C, Orlikowski D, Prigent H, Lacour A, Tard C, Furby A, et al. Effect of enzyme replacement therapy with alglucosidase alfa (Myozyme(R)) in 12 patients with advanced late-onset Pompe disease. Mol Genet Metab 2017;122(1-2):80–5.
[38] Prater SN, Banugaria SG, DeArmey SM, Botha EG, Stege EM, Case LE, et al. The emerging phenotype of long-term survivors with infantile Pompe disease. Genet Med 2012;14(9):800–10.
[39] Ebbink BJ, Poelman E, Aarsen FK, Plug I, Regal L, Muentjes C, et al. Classic infantile Pompe patients approaching adulthood: a cohort study on consequences for the brain. Dev Med Child Neurol 2018;60(6):579–86.
[40] Parenti G, Fecarotta S, la Marca G, Rossi B, Ascione S, Donati MA, et al. A chaperone enhances blood alpha-glucosidase activity in Pompe disease patients treated with enzyme replacement therapy. Mol Ther 2014;22(11):2004–12.
[41] Kishnani PS, Beckemeyer AA. New therapeutic approaches for Pompe disease: enzyme replacement therapy and beyond. Pediatr Endocrinol Rev 2014;12(Suppl 1):114–24.
[42] Heydemann A, Ceco E, Lim JE, Hadhazy M, Ryder P, Moran JL, et al. Latent TGF-beta-binding protein 4 modifies muscular dystrophy in mice. J Clin Invest 2009;119(12):3703–12.
[43] Roberts NW, Holley-Cuthrell J, Gonzalez-Vega M, Mull AJ, Heydemann A. Biochemical and functional comparisons of mdx and Sgcg(-/-) muscular dystrophy mouse models. Biomed Res Int 2015;2015:131436.
[44] Flanigan KM, Ceco E, Lamar KM, Kaminoh Y, Dunn DM, Mendell JR, et al. LTBP4 genotype predicts age of ambulatory loss in Duchenne muscular dystrophy. Ann Neurol 2013;73(4):481–8.
[45] van den Bergen JC, Hiller M, Bohringer S, Vijfhuizen L, Ginjaar HB, Chaouch A, et al. Validation of genetic modifiers for Duchenne muscular dystrophy: a multicentre study assessing SPP1 and LTBP4 variants. J Neurol Neurosurg Psychiatry 2015;86(10):1060–5.
[46] Weiss RB, Vieland VJ, Dunn DM, Kaminoh Y, Flanigan KM, United Dystrophinopathy P. Long-range genomic regulators of THBS1 and LTBP4 modify disease severity in duchenne muscular dystrophy. Ann Neurol 2018;84(2):234–45.
[47] Colella P, Sellier P, Costa Verdera H, Puzzo F, van Wittenberghe L, Guerchet N, et al. AAV gene transfer with tandem promoter design prevents anti-transgene immunity and provides persistent efficacy in neonate Pompe mice. Mol Ther Methods Clin Dev 2019;12:85–101.
[48] Cagin U, Puzzo F, Gomez MJ, Moya-Nilges M, Sellier P, Abad C, et al. Rescue of advanced Pompe disease in mice with hepatic expression of secretable acid alpha-glucosidase. Mol Ther 2020.
[49] Amalfitano A, McVie-Wylie AJ, Hu H, Dawson TL, Raben N, Plotz P, et al. Systemic correction of the muscle disorder glycogen storage disease type II after hepatic targeting of a modified adenovirus vector encoding human acid-alpha-glucosidase. Proc Natl Acad Sci USA 1999;96(16):8861–6.
[50] Spampanato C, Feeney E, Li L, Cardone M, Lim JA, Annunziata F, et al. Transcription factor EB (TFEB) is a new therapeutic target for Pompe disease. EMBO Mol Med 2013;5(5):691–706.
[51] Shoemaker JE, Lopes TJ, Ghosh S, Matsuoka Y, Kawaoka Y, Kitano H. CTen: a web-based platform for identifying enriched cell types from heterogeneous microarray data. BMC Genom 2012;13:460.
[52] Ayuso E, Mingozzi F, Production Bosch F. purification and characterization of adeno-associated vectors. Curr Gene Ther 2010;10(6):423–36.
[53] McGavern DB, Zoecklein L, Drescher KM, Rodriguez M. Quantitative assessment of neurologic deficits in a chronic progressive murine model of CNS demyelination. Exp Neurol 1999;158(1):171–81.
[54] Nascimbeni AC, Fanin M, Masiero E, Angelini C, Sandri M. The role of autophagy in the pathogenesis of glycogen storage disease type II (GSDII). Cell Death Differ 2012;19(10):1698–708.
[55] Klionsky DJ, Abdelmohsen K, Abe A, Abedin MJ, Abeliovich H, Acevedo Arozena A, et al. Guidelines for the use and interpretation of assays for monitoring autophagy (3rd edition). Autophagy 2016;12(1):1–222.
[56] Xu S, Lun Y, Frascella M, Garcia A, Soska R, Nair A, et al. Improved efficacy of a next-generation ERT in murine Pompe disease. JCI Insight 2019;4(5).
[57] Raben N, Wong A, Ralston E, Myerowitz R. Autophagy and mitochondria in Pompe disease: nothing is so new as what has long been forgotten. Am J Med Genet C Semin Med Genet 2012;160C(1):13–21.
[58] Lim JA, Li L, Kakhlon O, Myerowitz R, Raben N. Defects in calcium homeostasis and mitochondria can be reversed in Pompe disease. Autophagy 2015;11(2):385–402.
[59] Korlimarla A, Lim JA, Kishnani PS, Sun B. An emerging phenotype of central nervous system involvement in Pompe disease: from bench to bedside and beyond. Ann Transl Med 2019;7(13):289.
[60] Turner SMF, Falk DJ, Byrne BJ, Fuller DD. Transcriptome assessment of the Pompe (Gaa-/-) mouse spinal cord indicates widespread neuropathology. Physiol Genomics 2016;48(11):785–94.
[61] Smith BK, Corti M, Martin AD, Fuller DD, Byrne BJ. Altered activation of the diaphragm in late-onset Pompe disease. Respir Physiol Neurobiol 2016;222:11–5.
[62] van Putten M, Putker K, Overzier M, Adamzek WA, Pasteuning-Vuhman S, Plomp JJ, et al. Natural disease history of the D2-mdx mouse model for Duchenne muscular dystrophy. FASEB J 2019;33(7):8110–24.
[63] Raben N, Nagaraju K, Lee E, Plotz P. Modulation of disease severity in mice with targeted disruption of the acid alpha-glucosidase gene. Neuromuscul Disord 2000;10(4-5):283–91.
[64] Schiaffino S, Rossi AC, Smerdu V, Leinwand LA, Reggiani C. Developmental myosins: expression patterns and functional significance. Skelet Muscle 2015;5:22.
[65] Sandri M, El Meslemani AH, Sandri C, Schjerling P, Vissing K, Andersen JL, et al. Caspase 3 expression correlates with skeletal muscle apoptosis in Duchenne and facioscapulo human muscular dystrophy. A potential target for pharmacological treatment? J Neuropathol Exp Neurol 2001;60(3):302–12.
[66] Lagalice L, Pichon J, Gougeon E, Soussi S, Deniaud J, Ledevin M, et al. Satellite cells fail to contribute to muscle repair but are functional in Pompe disease (glycogenosis type II). Acta Neuropathol Commun 2018;6(1):116.
[67] Sahu A, Mamiya H, Shinde SN, Cheikhi A, Winter LL, Vo NV, et al. Age-related declines in alpha-Klotho drive progenitor cell mitochondrial dysfunction and impaired muscle regeneration. Nat Commun 2018;9(1):4859.

[68] Coley WD, Bogdanik L, Vila MC, Yu Q, Van Der Meulen JH, Rayavarapu S, et al. Effect of genetic background on the dystrophic phenotype in mdx mice. Hum Mol Genet 2016;25(1):130–45.
[69] Palermo AT, Palmer RE, So KS, Oba-Shinjo SM, Zhang M, Richards B, et al. Transcriptional response to GAA deficiency (Pompe disease) in infantile-onset patients. Mol Genet Metab 2012;106(3):287–300.
[70] Prater SN, Patel TT, Buckley AF, Mandel H, Vlodavski E, Banugaria SG, et al. Skeletal muscle pathology of infantile Pompe disease during long-term enzyme replacement therapy. Orphanet J Rare Dis 2013;8:90.
[71] Nelson CA, Hunter RB, Quigley LA, Girgenrath S, Weber WD, McCullough JA, et al. Inhibiting TGF-beta activity improves respiratory function in mdx mice. Am J Pathol 2011;178(6):2611–21.
[72] Caputo L, Granados A, Lenzi J, Rosa A, Ait-Si-Ali S, Puri PL, et al. Acute conversion of patient-derived Duchenne muscular dystrophy iPSC into myotubes reveals constitutive and inducible over-activation of TGFbeta-dependent pro-fibrotic signaling. Skelet Muscle 2020;10(1):13.
[73] Raben N, Danon M, Gilbert AL, Dwivedi S, Collins B, Thurberg BL, et al. Enzyme replacement therapy in the mouse model of Pompe disease. Mol Genet Metab 2003;80(1-2):159–69.
[74] Meena NK, Ralston E, Raben N, Puertollano R. Enzyme replacement therapy can reverse pathogenic cascade in Pompe disease. Mol Ther Methods Clin Dev 2020;18:199–214.
[75] Ribera A, Haurigot V, Garcia M, Marco S, Motas S, Villacampa P, et al. Biochemical, histological and functional correction of mucopolysaccharidosis type IIIB by intra-cerebrospinal fluid gene therapy. Hum Mol Genet 2015;24(7):2078–95.
[76] Motas S, Haurigot V, Garcia M, Marco S, Ribera A, Roca C, et al. CNS-directed gene therapy for the treatment of neurologic and somatic mucopolysaccharidosis type II (Hunter syndrome). JCI Insight 2016;1(9):e86696.
[77] Wootz H, Weber E, Korhonen L, Lindholm D. Altered distribution and levels of cathepsinD and cystatins in amyotrophic lateral sclerosis transgenic mice: possible roles in motor neuron survival. Neuroscience 2006;143(2):419–30.
[78] Vitner EB, Dekel H, Zigdon H, Shachar T, Farfel-Becker T, Eilam R, et al. Altered expression and distribution of cathepsins in neuronopathic forms of Gaucher disease and in other sphingolipidoses. Hum Mol Genet 2010;19(18):3583–90.
[79] Smith BK, Fuller DD, Martin AD, Lottenberg L, Islam S, Lawson LA, et al. Diaphragm pacing as a rehabilitative tool for patients with Pompe disease who are ventilator-dependent: case series. Phys Ther 2016;96(5):696–703.
[80] Ceco E, Bogdanovich S, Gardner B, Miller T, DeJesus A, Earley JU, et al. Targeting latent TGFbeta release in muscular dystrophy. Sci Transl Med 2014;6(259)259ra144.
[81] Lamar KM, Bogdanovich S, Gardner BB, Gao QQ, Miller T, Earley JU, et al. Overexpression of latent TGFbeta binding protein 4 in muscle ameliorates muscular dystrophy through Myostatin and TGFbeta. PLoS Genet 2016;12(5):e1006019.
[82] Juban G, Saclier M, Yacoub-Youssef H, Kernou A, Arnold L, Boisson C, et al. AMPK activation regulates LTBP4-dependent TGF-beta1 secretion by pro-inflammatory macrophages and controls fibrosis in Duchenne muscular dystrophy. Cell Rep 2018;25(8) 2163-76 e6.
[83] Mazala DA, Novak JS, Hogarth MW, Nearing M, Adusumalli P, Tully CB, et al. TGF-beta-driven muscle degeneration and failed regeneration underlie disease onset in a DMD mouse model. JCI Insight 2020;5(6).